

NAVAL POSTGRADUATE SCHOOL
Monterey, California



THESIS

**DETERMINING ENTRAINMENT RATE AND THE ROLE OF
ENTRAINMENT IN STRATOCUMULUS CLOUDS**

by

David W. McDowell

June 1999

Thesis Advisor:

Qing Wang

Approved for public release; distribution is unlimited.

19990818 279

REPORT DOCUMENTATION PAGE			Form Approved OMB No. 0704-0188	
Public reporting burden for this collection of information is estimated to average 1 hour per response, including the time for reviewing instructions, searching existing sources, gathering and maintaining the data needed, and completing and reviewing the collection of information. Send comments regarding this burden estimate or any other aspect of this collection of information, including suggestions for reducing this burden to Washington Headquarters Services, Directorate for Information Operations and Reports, 1215 Jefferson Davis Highway Suite 1204, Arlington, VA 22202-4312, and to the Office of Management and Budget, Paperwork Reduction Project (0704-0188), Washington, DC 20503.				
1. AGENCY USE ONLY (Leave blank)	2. REPORT DATE June 1999	3. REPORT TYPE AND DATES COVERED Master's Thesis		
4. TITLE AND SUBTITLE DETERMINING ENTRAINMENT RATE AND THE ROLE OF ENTRAINMENT IN STRATOCUMULUS CLOUDS			5. FUNDING NUMBERS	
6. AUTHOR(S) David W. McDowell				
7. PERFORMING ORGANIZATION NAME(S) AND ADDRESS(ES) Naval Postgraduate School Monterey, CA 93943-5000			8. PERFORMING ORGANIZATION REPORT NUMBER	
9. SPONSORING/MONITORING AGENCY NAME(S) AND ADDRESS(ES)			10. SPONSORING/MONITORING AGENCY REPORT NUMBER	
11. SUPPLEMENTARY NOTES The views expressed in this thesis are those of the author and do not reflect the official policy or position of the Department of Defense or the U.S. Government.				
12a. DISTRIBUTION/AVAILABILITY STATEMENT Approved for public release; distribution is unlimited.			12b. DISTRIBUTION CODE	
13. ABSTRACT (Maximum 200 words) An important process in predicting the evolution of the boundary layer is the entrainment rate, which has received little verification using observed data. The entrainment rate is therefore computed using aircraft measurements obtained off the coast of California during FIRE in 1987. The entrainment zone is defined and determined to be typically less than 10 meters deep. The structure above the boundary layer is found very complex and consists of a layered structure located in the first few hundred meters above the cloud top. These layers are 20-130 meters deep and possess properties that relate the layers to boundary layer processes. A conceptual model is presented to explain the formation of these layers. The added presence of the layered structure above the cloud top complicates the determination of jump conditions and thus the calculation of entrainment velocity. In addition, jumps in conserved quantities vary considerably between soundings, which questions the validity of using a simple average to calculate the entrainment rate. Therefore, a new method for calculating entrainment velocity is presented, which decreases the variation in jump conditions. This method is physically based and yields an entrainment rate with significantly less uncertainty.				
14. SUBJECT TERMS Entrainment, entrainment rate, stratocumulus, boundary layer, FIRE			15. NUMBER OF PAGES 78	
			16. PRICE CODE	
17. SECURITY CLASSIFICATION OF REPORT Unclassified	18. SECURITY CLASSIFICATION OF THIS PAGE Unclassified	18. SECURITY CLASSIFICATION OF ABSTRACT Unclassified	20. LIMITATION OF ABSTRACT UL	

NSN 7540-01-280-5500

Standard Form 298 (Rev 2-89)
Prescribed by ANSI Std. Z39-18
298-102

Approved for public release; distribution is unlimited

**DETERMINING ENTRAINMENT RATE AND THE ROLE OF ENTRAINMENT IN
STRATOCUMULUS CLOUDS**

David W. McDowell
Lieutenant, United States Navy
B.S., University of Washington, 1990

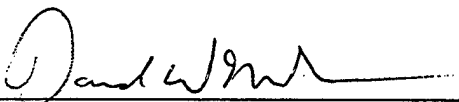
Submitted in partial fulfillment of the
requirements for the degree of

**MASTER OF SCIENCE IN METEOROLOGY AND
PHYSICAL OCEANOGRAPHY**

from the

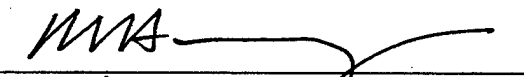
**NAVAL POSTGRADUATE SCHOOL
June 1999**

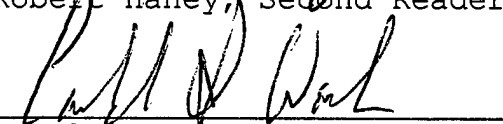
Author:


David W. McDowell

Approved by:


Qing Wang, Thesis Advisor


Robert Haney, Second Reader


Carlyle H. Wash, Chairman,
Department of Meteorology

ABSTRACT

An important process in predicting the evolution of the boundary layer is the entrainment rate, which has received little verification using observed data. The entrainment rate is therefore computed using aircraft measurements obtained off the coast of California during FIRE in 1987. The entrainment zone is defined and determined to be typically less than 10 meters deep. The structure above the boundary layer is found very complex and consists of a layered structure located in the first few hundred meters above the cloud top. These layers are 20-130 meters deep and possess properties that relate the layers to boundary layer processes. A conceptual model is presented to explain the formation of these layers.

The added presence of the layered structure above the cloud top complicates the determination of jump conditions and thus the calculation of entrainment velocity. In addition, jumps in conserved quantities vary considerably between soundings, which questions the validity of using a simple average to calculate the entrainment rate. Therefore, a new method for calculating entrainment velocity is presented, which decreases the variation in jump conditions. This method is physically based and yields an entrainment rate with significantly less uncertainty.

TABLE OF CONTENTS

I.	INTRODUCTION	1
II.	BACKGROUND ON ENTRAINMENT AND ENTRAINMENT RATE	7
	A. STRATOCUMULUS-TOPPED BOUNDARY LAYERS	7
	B. ENTRAINMENT AND THE ENTRAINMENT ZONE	9
	1. Entrainment	9
	2. The Entrainment Zone	10
	C. ENTRAINMENT RATE	13
III.	DATA	15
	A. OVERVIEW OF EXPERIMENT	15
	B. AIRCRAFT AND INSTRUMENTATION	17
	1. Aircraft	17
	2. Instrumentation	18
	C. DETERMINATION OF ENTRAINMENT FLUXES	20
IV.	JUMP CONDITION VARIABILITY AND LAYERED STRUCTURE ABOVE THE BOUNDARY LAYER	25
	A. DETERMINATION OF JUMP CONDITIONS	25
	B. LAYERED STRUCTURE ABOVE THE ENTRAINMENT ZONE ..	31
	C. HYPOTHESIS ON FORMATION OF LAYERED STRUCTURE ..	34
	1. Entrainment Drying	34
	2. Other Possibilities	43
V.	ENTRAINMENT VELOCITY	45
	A. ENTRAINMENT VELOCITY VARIABILITY	45
	B. AN ALTERNATE METHOD FOR CALCULATING ENTRAINMENT VELOCITY	49

VI. SUMMARY, CONCLUSIONS, AND DISCUSSION	57
A. SUMMARY AND CONCLUSIONS	57
B. DISCUSSION	60
LIST OF REFERENCES	63
INITIAL DISTRIBUTION LIST	67

ACKNOWLEDGEMENTS

I would like to thank my advisor, Dr. Qing Wang, of the Department of Meteorology, Naval Postgraduate School, for her guidance and support during the development of this thesis. Her comments and discussions on entrainment and boundary layer structure were the backbone of this study. Additionally, I would like to thank Dr. Robert Haney for his helpful comments as the second reader.

I also thank the following people for their direct and/or indirect support during this endeavor: Mr. Kurt Nielsen, Mary Jordan, Russ Schwanz, Bob Creasey, and Dick Lind. I would especially like to thank my wife, Dianna, and sons, Benjamin and Thomas, for their loving support and patience during the writing of this thesis.

I. INTRODUCTION

The structure and evolution of the cloud-topped boundary layer are of significant meteorological interest and of tactical importance to the United States Navy. In contrast to a cloudless boundary layer, a boundary layer topped with extensive clouds, such as stratocumulus, adds a level of complexity and uncertainty in the ability to assess or even predict boundary layer structure. As a result, weather forecasts and the effectiveness of tactical decisions may be degraded. The presence of stratocumulus, for example, significantly alters the boundary layer inversion strength, which plays a role in Electromagnetic and Electro Optical propagation and the tactical use of elevated ducts. The change in inversion stability and corresponding changes in cloud evolution also modifies aerosol-cloud interaction. The resulting changes to cloud structure therefore impact Navy remote sensing and surveillance capability, such as in the satellite analysis of ship tracks. In addition, the presence of stratocumulus adds difficulty to short-period and mesoscale forecasting, pollution transport and its chemical evolution, and radiative feedback processes in climate studies. Consequently, an improved understanding of the evolution of a stratocumulus-topped boundary layer could significantly enhance the Navy's tactical use of the environment.

One important process in the evolution of a stratocumulus-topped boundary layer is entrainment, which describes the exchange process between the relatively quiescent free atmosphere and the turbulent boundary layer.

Entrainment, or more importantly the rate of entrainment, transports free tropospheric air into the cloud-topped boundary layer. The resulting mixing then alters cloud structure and consequently influences the boundary layer dynamics and thus boundary layer structure. A quantitative measure of the rate of entrainment, or entrainment velocity, is therefore essential in determining low-level cloud evolution. The objective of this thesis, then, is to evaluate a reliable means of quantifying entrainment velocity.

Many attempts have been made in the past to infer the physical processes that drive entrainment; however, a consensus regarding the interaction between the myriad of individual processes has not been reached. Consequently, the process of entrainment and the physical processes that potentially modify the effects of entrainment are poorly understood. The role of entrainment in the mixing process, for example, has received much attention. Nicholls and Turton (1986), for instance, have shown that significant mixing occurs in a relatively shallow layer of only a few tens of meters deep. In their analysis, they conclude that filaments of relatively subsaturated and warm air are drawn from the shallow layer into the boundary layer by turbulent motion. The downdrafts then mix into the cloud layer, whereby evaporative cooling generates turbulent kinetic energy (TKE) as the cooled cloud parcels become negatively buoyant and sink. This process, which relates entrainment mixing to the downward acceleration of mixed parcels, is the basis for early studies of cloud-top entrainment instability (CTEI) (Randall, 1980). It emphasizes the positive feedback between negative buoyancy produced by evaporative cooling and the generation of TKE.

The significance of the role of evaporative cooling, however, has also been questioned. Some studies, for example, describe CTEI as an interfacial instability, whereby entrainment driven evaporative cooling dominates all other physical processes in the generation of TKE (Randall, 1980; MacVean and Mason, 1990; Siems et al., 1990). Furthermore, Siems et al. (1990) points out that typical cloud top jump conditions do not satisfy the criteria for strong buoyancy reversal and are not consistent with the rapidly induced entrainment normally observed in the real stratocumulus topped boundary layer. Nicholls (1989) further shows that evaporation alone cannot produce the negative buoyancy which is typically observed. Nicholls and Turton (1986) estimate that other factors, such as latent heat release and radiative cooling, may dominate over the effects of evaporative cooling. They conclude that radiative cooling effects are more significant than the effects of evaporative cooling when little mixing occurs.

In another perspective on entrainment and the mechanisms which determine the rate of entrainment, the interaction between entrainment and the boundary layer circulation has been investigated (e.g., Albrecht et al., 1985; Moeng et al., 1992; Wang and Albrecht, 1994). These studies show that entrainment is enhanced by evaporative cooling through the boundary layer circulation (Albrecht et al., 1985). A conceptual model (Wang and Albrecht, 1994) suggests evaporative cooling and radiative cooling together result in the downward acceleration of the mixture. The excess buoyancy flux in the entrainment downdrafts then serves to maintain or strengthen the boundary layer circulation. In return, the stronger boundary layer circulation can then increase the entrainment.

An important aspect of entrainment is the role of entrainment mixing in the structure of the stratocumulus cloud layer. Since one effect of entrainment is to transfer above boundary layer air properties into the cloud layer, the entrainment velocity and the specific properties of the above inversion air play an important role in determining the cloud microphysics. Latham and Reed (1977) suggest that evaporation caused by the entrainment of dry inversion air into the boundary layer results in a reduction in droplets of all sizes through the inhomogeneous mixing process. Their theory suggests a reduction in droplet concentration rather than a reduction in the mean droplet size. Another effect of entrainment is to modify the concentration of cloud condensation nuclei (CCN) since the condensation nuclei in the entrained air are unlikely to be activated at the cloud top (Nicholls and Leighton, 1986). This suggests that mixing of dry air into the boundary layer affects the formation of some new droplets. An in-depth understanding regarding the effects of entrainment therefore provides insight towards stratocumulus cloud evolution.

In the past decade, several extensive field measurements have occurred to increase our understanding of stratocumulus-topped boundary layer processes. These measurements, from experiments like the First International Satellite Cloud and Climatology Project (ISCCP) Experiment (FIRE), the Atlantic Stratocumulus Transition Experiment (ASTEX), and the Monterey Area Ship Tracks (MAST) experiment, have significantly enhanced our knowledge of important physical process such as decoupling, cloud-top entrainment instability (CTEI), cumulus-stratocumulus interaction, and cloud-aerosol interaction. However, the entrainment rate in a stratocumulus-topped boundary layer

remains a significant unknown. For example, Moeng et al. (1998) examines the current capability of representing the stratocumulus-topped boundary layer in numerical models by comparing results from various large eddy simulation (LES) and 1-D models. Moeng et al. (1998) concludes that differences between the participating LES models exist as a result of different entrainment rates. The calculation of the entrainment rate has thus become a central issue in stratocumulus-topped boundary layer studies.

The major difficulty in the study of the entrainment rate from observations is the uncertainty in determining its value. The uncertainty is mainly a result of variability in the jump conditions, which are determined from individual soundings. In this study, the detailed structure of the above boundary layer air is analyzed in an effort to understand the variability of the jump conditions. A new method for determining entrainment velocity is also developed and tested. This new method is physically based and yields an entrainment rate with significantly less uncertainty. The reliability of the method is evaluated using aircraft measurements obtained off the coast of California during FIRE in 1987. A major objective of this analysis is to understand the structure near the cloud top and to develop an optimal method for determining entrainment velocity.

This thesis is organized into seven chapters. Chapter II describes the basic background behind describing entrainment and the rate of entrainment in a marine atmospheric boundary layer topped with stratocumulus. Chapter III describes the data used in the calculation of entrainment velocity. Chapter IV provides a detailed analysis of the entrainment zone and the above boundary

layer structure. Chapter V presents the new method for calculating entrainment velocity. Discussion and conclusions are offered in Chapter VI. Finally, Chapter V gives recommendations for further research.

II. BACKGROUND ON ENTRAINMENT AND ENTRAINMENT RATE

A. STRATOCUMULUS-TOPPED BOUNDARY LAYERS (STBL)

The presence of stratocumulus clouds, in contrast to a clear atmospheric boundary layer (ABL), adds a level of complexity to boundary layer structure and the physical processes that drive boundary layer dynamics. Additional factors that must now be considered include the radiative fluxes and phase changes associated with the presence of a stratocumulus cloud deck. Whereas surface fluxes and large-scale external conditions drive the turbulence structure of the dry ABL (Garratt, 1992), radiation fluxes which produce local heating or cooling within the boundary layer must be included when the boundary layer is cloud topped. In addition, phase changes may alter the turbulent kinetic energy (TKE) budget through evaporative cooling. Deardorff (1980) and Randall (1980) have investigated the thermodynamics and significance of this cloud top evaporative cooling effect.

The mechanisms that determine the dynamics of the STBL can be explored by considering the possible sources of TKE. Knowledge of turbulence structure and mixing processes then lead to valuable insights into the cloud microphysics and the possible role of entrainment in determining cloud structure. Numerous studies in the past have revealed information regarding the detailed structure of the marine STBL off the southern California coast.

In 1976 during the Marine Stratocumulus Experiment (STRATEX) off the southern California coast, Brost et al. (1982) and Albrecht et al. (1985) analyzed aircraft data

consisting of well-mixed boundary layer cases. Brost et al. (1982) concluded that shear production played an important role in the TKE budget at that time. Penc and Albrecht (1987) later determined that two of the cases studied by Brost et al. (1982) were also influenced by large surface buoyancy flux with large variability in the in-cloud buoyancy flux. As a contrast, Hignett (1991) studied tethered balloon observations on San Nicolas Island during FIRE. He encountered strong diurnal variations in turbulent mixing and estimated that cloud-top radiative cooling was the major source of TKE. Hignett (1991) also concluded that boundary layer turbulence structure was determined mostly by in-cloud buoyancy flux and differential warming of the boundary layer.

All of these studies suggest that a variety of boundary layers, each with a unique turbulence structure, can exist at different times in the same region. It is therefore important to possess a detailed knowledge of the turbulent transport and mixing processes that reflect the true boundary layer dynamics. Wang (1993) provides such information, whereby the key physical processes are analyzed. The motivation for this thesis is to understand the cloud top entrainment process and to develop a reliable calculation for entrainment velocity, which will describe the interaction of these physical processes and their net effect on entrainment.

B. ENTRAINMENT AND THE ENTRAINMENT ZONE

1. Entrainment

Entrainment is the process whereby fluid is exchanged across a density interface bounding a region of turbulent flow. This exchange process physically occurs when turbulent motions engulf a relatively quiescent fluid across the mean density interface such that the quiescent fluid is mixed into the turbulent region. Smaller scale motion is rapidly damped by the interfacial density gradient and the volume of the turbulent region increases (Nicholls and Turton, 1986). Turner (1973) developed this description of the entrainment process in laboratory experiments. A transformation to its application in an observed stratocumulus-topped boundary layer can be made by relating the density interface to the base of the inversion and the interfacial density gradient to the strength of the inversion. In this respect, entrainment entails the transport of above boundary layer air properties into the boundary layer via turbulent motion. The ensuing boundary layer mixing between the above boundary layer air properties and the cloud layer properties can then change the cloud microphysics. The degree of this change in cloud microstructure depends not only on the boundary layer turbulence structure (i.e. dynamics) and the properties of the air above the boundary layer, but also on the degree of mixing determined by the entrainment process.

2. The Entrainment Zone

Numerous past studies have yielded significant results regarding the understanding of entrainment in a clear convective boundary layer. Deardorff et al. (1979) provided an early description of entrainment zone in a convectively mixed layer by performing experiments in a laboratory convection chamber. From this, he defined the entrainment zone as the outermost portion of the mixed layer where non-turbulent fluid is being entrained, but is not yet incorporated into the well-mixed layer. The top of the entrainment zone was therefore determined to be the maximum height any mixed parcel could reach. His depiction of the entrainment zone is shown in Figure 1, where the depth marked Δh is an ensemble-mean of many soundings. Tank study results indicated that the depth of the entrainment zone was typically 25% of the mixed layer depth, but



Figure 1 Depiction of the Entrainment Zone in a Convection Tank, from Deardorff et al. (1979). Light areas show the well mixed fluid. The region indicated by Δh is defined as the entrainment zone.

Deardorff (1979) suggested that the actual thickness of the entrainment zone was difficult to determine. He concluded that knowledge of the thickness of the entrainment zone was essential for developing and testing mixed layer growth theories.

Similar to research conducted for the clear convective boundary layer, other studies have analyzed the structure of the entrainment zone for boundary layers topped by stratocumulus clouds. Measurements analyzed by Nicholls and Turton (1986), for example, indicated a thin layer of only a few meters deep, in which significant mixing of cloudy and inversion air occurred. This region was described as the entrainment interface layer (EIL) following Caughey et al. (1982), which differs from the definition developed by Deardorff for the clear case. In their definition, Caughey et al. (1982) defined the upper extent of the entrainment zone as the depth at which turbulent vertical velocity fluctuations extend above a sharply defined inversion base. In contrast to the clear case, the EIL was found to have a characteristic entrainment scale of about 10m (Caughey et al., 1982). Nicholls and Turton (1986) found similar results for the EIL and suggested that entrainment in this zone occurs as an interfacial process in a smaller layer compared to the description given by Deardorff. (1980). In their study of the EIL, Nicholls and Turton noticed that total water and virtual potential temperature were negatively correlated and suggested that the interfacial density jump across the layer was modified by physical processes occurring within the entrainment region. In situ processes, such as radiative and evaporative cooling were therefore determined to be an additional source of density fluctuations, in addition to the processes known to

affect entrainment in cloud-free situations. These additional factors were found to result in an entrainment rate 4 to 13 times the value determined for similar cloud-free conditions.

The differences found in the definitions and observed structure of the entrainment zone between cloud-free and stratocumulus topped boundary layers suggest a need for an increased understanding of entrainment under cloudy conditions. The changes that occur to the inversion and

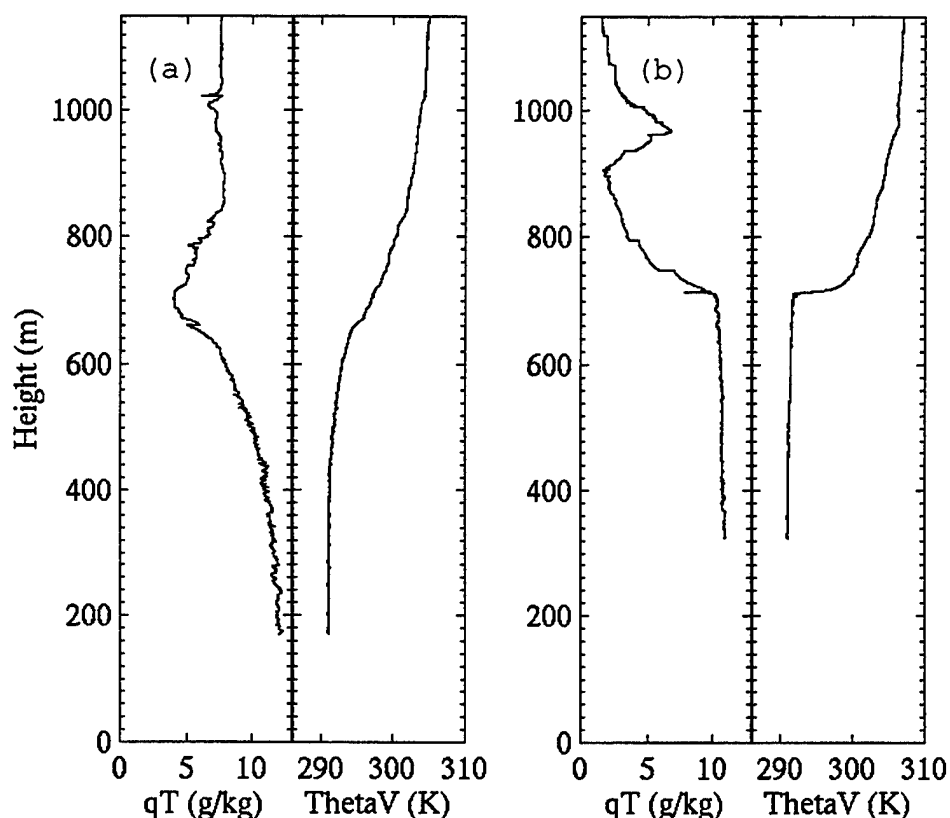


Figure 2 Comparison Between a Cloud-topped and Clear Boundary Layer from Flight 5 of FIRE. Total water and virtual potential temperature profiles for the clear case are shown in (a) and for the stratocumulus-topped case in (b).

entrainment zone structure when clouds are present do not appear subtle. An example of the added complexity due to the presence of stratocumulus is shown in Figure 2. This comparison between two soundings taken from the same area on the same day demonstrates the significant changes that can occur when clouds are present. The strengthening of the inversion in the stratocumulus topped boundary layer profile suggests the added effect of radiative cooling at the cloud top. With these types of observed differences, more detail regarding the entrainment process in a stratocumulus-topped boundary layer is needed if the effect of such clouds on boundary layer evolution is to be fully understood.

C. ENTRAINMENT RATE

The role of entrainment and the determination of the entrainment rate are undoubtedly complex issues. They are, however, essential elements in predicting cloud and boundary layer evolution. Since entrainment transports air from above the boundary layer into the cloud layer, the entrainment rate therefore quantifies the rate of exchange, or flux, across the inversion. Characteristics of the entrainment rate, along with the properties of the above inversion air, are fundamental towards interpreting the interaction of the key physical boundary layer processes. A reliable method for calculating entrainment velocity is therefore essential if the effects of entrainment on boundary layer structure are to be analyzed.

The entrainment rate is defined by Deardorff (1976) as,

$$w_e = -\frac{\overline{w'\phi'}}{\Delta\phi}, \quad (1)$$

where ϕ is any conserved variable and $\Delta\phi$ is an ensemble-mean of the jump conditions across the entrainment zone. This definition is used in this thesis to calculate the entrainment velocity using total water and ozone. The objective of performing the calculation is to understand the result and to gain insight into the improvement of parameterizations of entrainment rate for stratocumulus topped boundary layers.

III. DATA

A. OVERVIEW OF EXPERIMENT

On 29 June - 19 July 1987 the First International Satellite Cloud and Climate Project (ISCCP) Regional Experiment (FIRE) completed the Marine Stratocumulus Intensive Field Observations (IFO) phase off the coast of southern California. Using 12 coordinated multi-missions with five separate research aircraft and a collection of surface-based measurements and satellite imagery, one objective of FIRE was to bridge together the interaction between physical processes of varying scales in terms of the structure and evolution of stratocumulus clouds. The aim of this objective was to increase the understanding of stratocumulus development, maintenance, and dissipation and to use this knowledge to improve parameterizations used in large-scale models and to assess methods for remote sensing of cloud properties. A detailed description of project objectives is given in Albrecht et al. (1988) and Cox et al. (1987). In addition, Kloesel et al. (1988) gives a summary of experiment operations and general meteorological conditions during the period. In this study, observations provided by the NCAR Electra aircraft are exclusively used to analyze the turbulence and inversion structure of the cloudy boundary layer. The general locations of each of the nine Electra flights are shown in Figure 3. Figure 4 depicts the typical stratocumulus cloud cover experienced during the experiment.

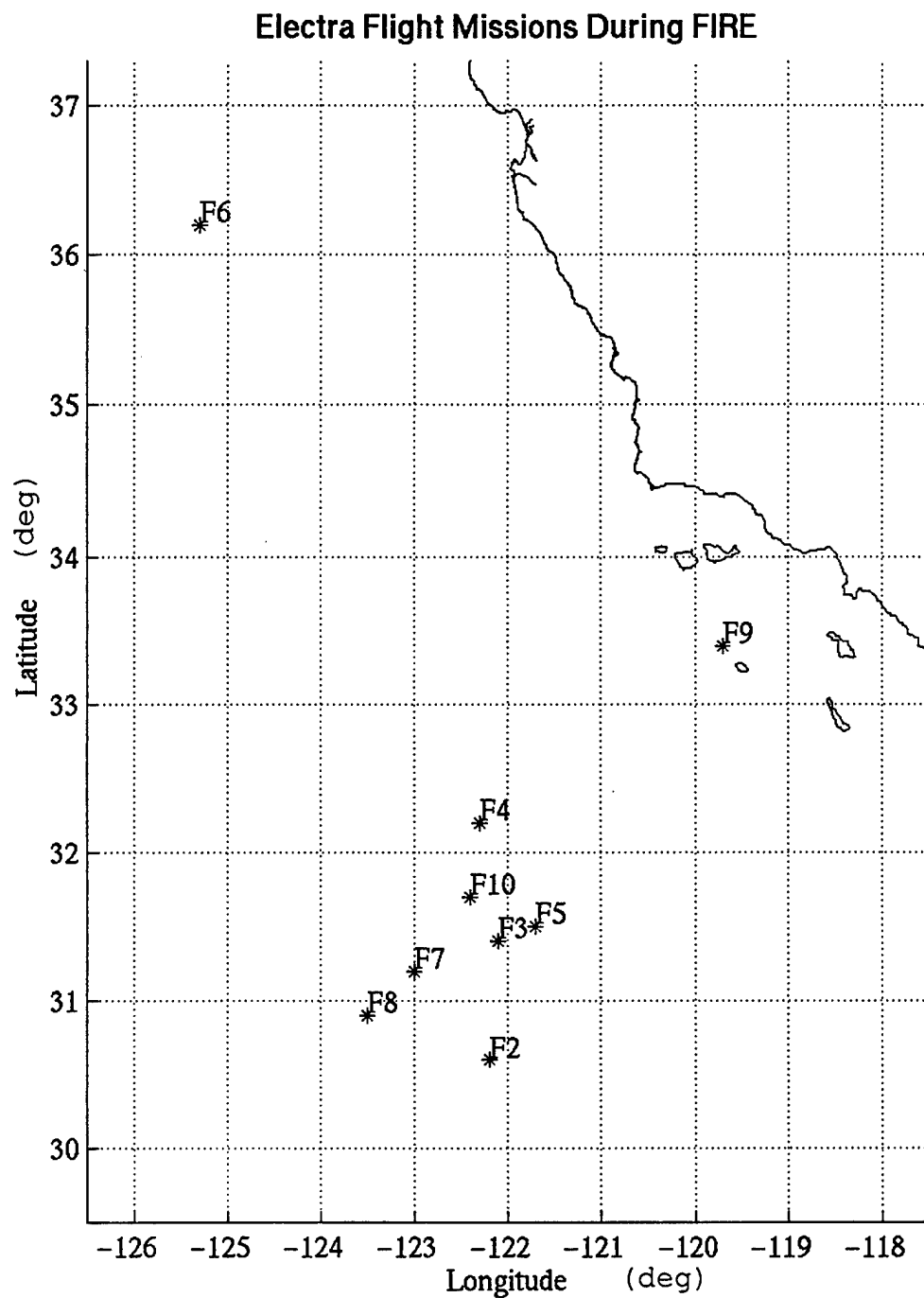


Figure 3 Flight Missions Flown by Electra During FIRE. Positions indicate the center of each region covered during the respective Electra flights. The solid lines denote the coastline.

B. AIRCRAFT AND INSTRUMENTATION

1. Aircraft

The National Center for Atmospheric Research (NCAR) Electra aircraft was used to characterize the turbulence, radiation, and cloud microphysics characteristics of the boundary layer. Each Electra mission consisted of horizontal flight legs at constant headings and slant path or spiral soundings at multiple time periods and locations.

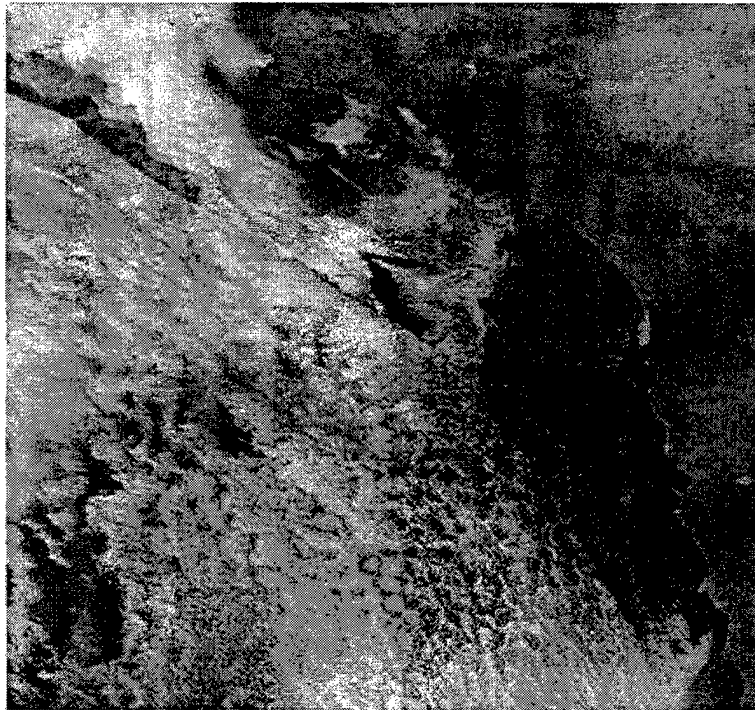


Figure 4 Stratocumulus Cloud Cover on June 25, 1987. The extent of cloud cover reflects the typical cloud conditions experienced during FIRE.

The aircraft speed was held constant at 100 m/s. Horizontal flight legs consisted of 10-20 minute legs at levels below, in and above the cloud layer, to capture cloud structure and to measure the turbulent flux at various levels in the boundary layer. Temporal variations within each flight were considered negligible. Wang (1993) suggested that time variations in the boundary layer turbulent structure were small given the uncertainties in the turbulence statistics. Aircraft soundings provided vertical profiles of boundary layer variations, inversion layer characteristics, and a representation of the above boundary layer air properties. Aircraft soundings were treated as vertical profiles assuming near horizontal homogeneity.

2. Instrumentation

Temperature variations were obtained using a Rosemount Type 102 sensor located on the boom of the aircraft. Betts and Boers (1990) estimated that this thermal sensor was least affected by wetting in the cloud layer. Virtual potential temperature was derived from temperature and specific humidity measurements using methods described by Bolton (1980) and Buck (1981).

Moisture variations were captured as absolute humidity at a high sampling rate using a Lyman-Alpha hygrometer calibrated by a dew-point hygrometer. Paluch and Lenschow (1991) estimated that these moisture measurements might be over-estimated by a few tenths of a gram per kilogram. However, this error in the absolute measurement is not a significant factor in moisture flux calculation and the determination of the cloud-top moisture jump conditions.

The calibrated Lyman-Alpha measurements are therefore used in this thesis to calculate moisture flux and to illustrate the boundary layer moisture structure.

Fast response ozone measurements were obtained using a Model Mark II sensor. The high-rate ozone mixing ratio was determined using the nitric oxide-chemiluminescence method discussed in Albrecht et al. (1988). The fast ozone measurements are used in this study to determine the ozone cloud-top jump conditions across the entrainment zone and the ozone flux in the upper boundary layer.

Liquid water variations were measured by a King Liquid Water Probe at a high sample rate. Betts and Boers (1990) showed that the King Probe provided fewer variable offset errors compared to other available liquid water sensors. They estimated that the typical liquid water measurement errors could be $\pm 50\%$ with a tendency for liquid water to be underestimated. In addition to the King Probe, the Particle Measuring Systems (PMS) Inc. Model Forward Scattering Spectrometer Probe (FSSP) - 100 measured droplet size spectra for droplet sizes of 3-45 microns. In this study, the King Probe measurements are used for cloud liquid water content and the FSSP for droplet concentration and size distribution.

C. DETERMINATION OF ENTRAINMENT FLUXES

Entrainment fluxes of moisture, equivalent potential temperature, and ozone were determined using the eddy correlation method. In this process, cospectra of vertical velocity and either moisture, equivalent potential

temperature, or ozone were obtained using the Fast Fourier Transform (FFT) method. The cospectra were then integrated from the smallest resolvable scale to a large wavelength cutoff to eliminate the large-scale and mesoscale influence not sufficiently sampled by the aircraft measurements. Paluch and Lenschow (1991) noted that turbulence statistics obtained by filtering out variations greater than 5km in the FIRE data produced results similar to when a 2km high pass filter was applied. This suggests that the spectral gap in the kinetic energy spectrum (Stull, 1988) could be on the order of 5km. In this particular study, a wavelength cutoff of 6km was chosen to separate the microscale turbulence from the mesoscale and synoptic scale variations.

Wang (1993) pointed out that there are two primary sources of error in computing the turbulence statistics: error due to instrument response and error associated with the length and time of the statistical sample record. Errors associated with instrument response are purely a function of instrument technology and can only improve with technological advancements. Error due to the length and time of the sample, however, can be minimized by increasing the record length and by decreasing the temporal variability aspect of the measured quantity. In this analysis, typical horizontal legs measured 10 minutes or 60km in length. Some in-cloud flux legs required the removal of clear patches to compute the in-cloud turbulent statistics. In these cases, horizontal legs decreased below a 30km or a 5 minute record length were not included in the boundary layer flux profiles in order to maintain statistical significance in the flux values. The typical time span between the horizontal flight legs and soundings used in the analysis for each flight was

4-5 hours. Changes in the boundary layer structure within this time period were considered negligible.

Vertical profiles of moisture, equivalent potential temperature, and ozone flux were constructed using a linear approximation in the upper boundary layer. A linear fit assumes that temporal changes in the vertical gradient of the mean quantities of moisture and ozone are negligible (Garratt, 1992). For a well-mixed layer, the vertical flux profile of a conserved variable is expected to be linear with height through the depth of the layer. This is generally the case, as shown in Figure 5. In this analysis, entrainment fluxes were determined using the best fit linear profile from measurements in the cloud mixed layer. In a well-mixed boundary layer, the cloud mixed layer is the entire boundary layer, while in a decoupled boundary layer the cloud mixed layer is the upper layer associated with the cloud layer (Wang 1993). Cloud top heights were obtained using LIDAR measurements or sounding profiles when LIDAR measurements were not available. Figure 5 and Figure 6 show examples of the flux profiles and the linear best fit for two of the Electra flights. In addition, Table 1 gives the estimated flux values for moisture and ozone at the cloud top for all nine flights.

Table 1 Estimated entrainment fluxes for ozone and total water. Units are $\text{ms}^{-1}\text{ppbv}$ for ozone flux and W/m^2 for total water flux.

Flight	$\overline{w'O_3'}$	$\rho L \overline{w'q'}$
2	-.01	28.7
3	-.10	58.9
4	-.03	34.1
5	.04	45.8
6	.01	8.0
7	-.02	13.6
8	.01	32.0
9	-.20	13.0
10	-.03	42.2

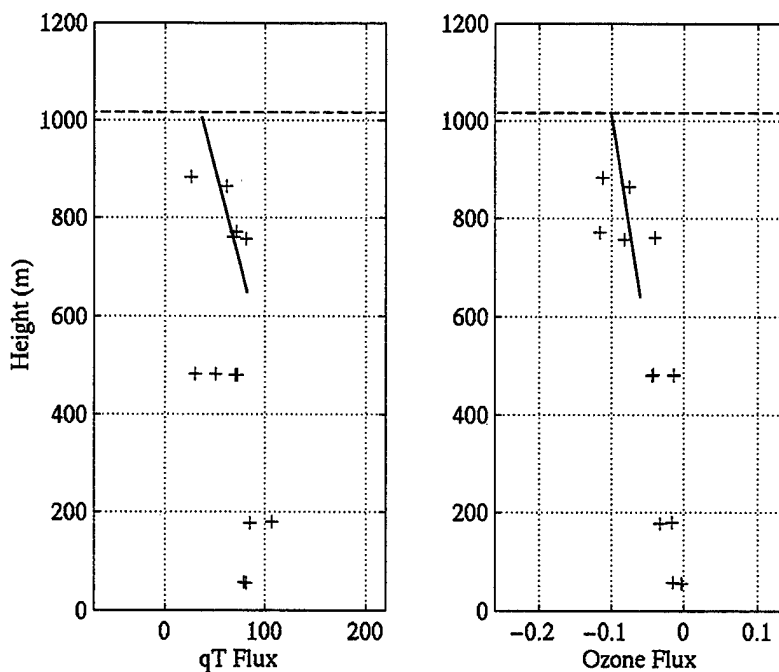


Figure 5 Flight 3 Flux Profiles for Ozone and Total Water. Units are $\text{ms}^{-1}\text{ppbv}$ for ozone flux and W/m^2 for total water flux. The dashed line indicates the average cloud top.

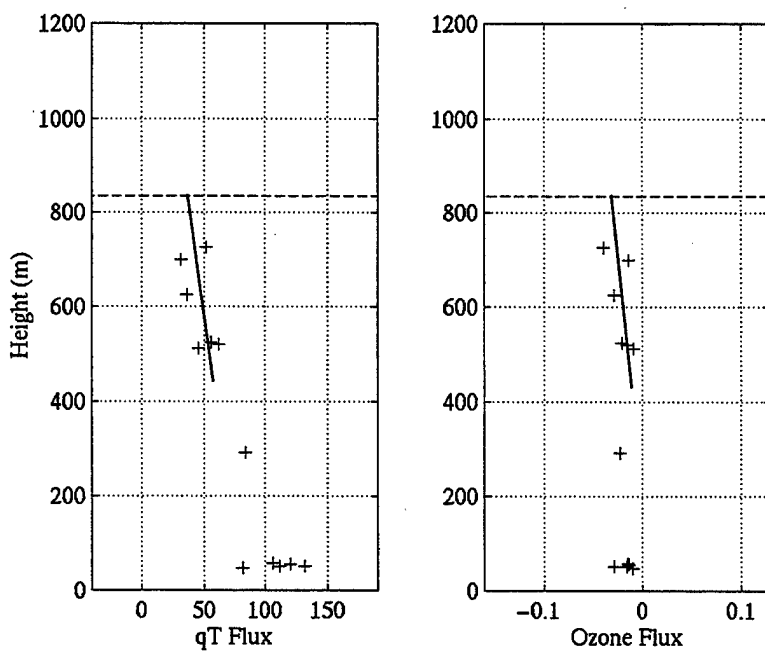


Figure 6 Same as in Figure 5, except for Flight 4.

IV. JUMP CONDITION VARIABILITY AND LAYERED STRUCTURE ABOVE THE BOUNDARY LAYER

A. DETERMINATION OF JUMP CONDITIONS

Jump conditions were estimated using aircraft soundings. Vertical profiles of total water, virtual potential temperature, and ozone were first analyzed to identify the top of the cloud mixed layer. Mean FSSP droplet concentrations were added to identify the vertical extent of the stratocumulus cloud layer. In addition, a multi-level 1-D wavelet decomposition of vertical velocity and potential temperature were utilized to evaluate the vertical extent of turbulence and mixing. This application of the wavelet analysis has been discussed in Wang et al. (1998). In general, the top of the mixed layer correlated well with the cloud top, as indicated by the droplet concentration, and with the region of uniform turbulence and mixing, as indicated from the wavelet analysis profiles. The top of the well-mixed region also corresponded very well with the inversion base, above which gradients in some observed quantities were found. As a result, the height of the inversion layer base and corresponding total water and ozone values were determined using the height at the cloud top which still reflected well-mixed conditions. Total water was computed as the sum of water vapor and liquid water ($q_T = q_v + q_l$).

The inversion top was determined using the height at which the initial gradients of virtual potential temperature, total water, and ozone quickly decreased with height. The depth of the strong gradient layer was

typically the same for virtual potential temperature and total water, whereby the end of the initial virtual potential temperature increase correlated well with the end of the initial total water decrease. The layer selected to represent the inversion layer was therefore chosen as this strong gradient layer in direct contact with the mixed layer. It was noted that some soundings revealed a lag in instrument response for ozone, which resulted in an often deeper mixed layer as described by the high-rate sampled ozone. This might have been caused by the TECO ozone sensor that was used to calibrate the absolute chemiluminescent fast ozone measurements. Consequently, the inversion base and the inversion top heights were not always the same for ozone as for the other conserved variables. The same initial gradient layer as that found in the virtual potential temperature and ozone profiles was, however, still observed above the ozone indicated mixed layer.

The layer immediately above the cloud top is of particular interest in this study since entrainment of the layer properties exerts direct influence on the dynamics and thermodynamics of the boundary layer (Wang, 1993). The upper bounds for the jump conditions were thus obtained using the values of total water, virtual potential temperature, and ozone at the top of the inversion layer residing immediately above the mixed layer. Changes in virtual potential temperature, total water, and ozone across the inversion layer (termed inversion jumps) were then calculated using the difference between the conserved values at the upper and lower bounds to the inversion layer. The vertical profiles from soundings from Flight 4 (Figure 7) demonstrate the typical properties of the inversion layer.

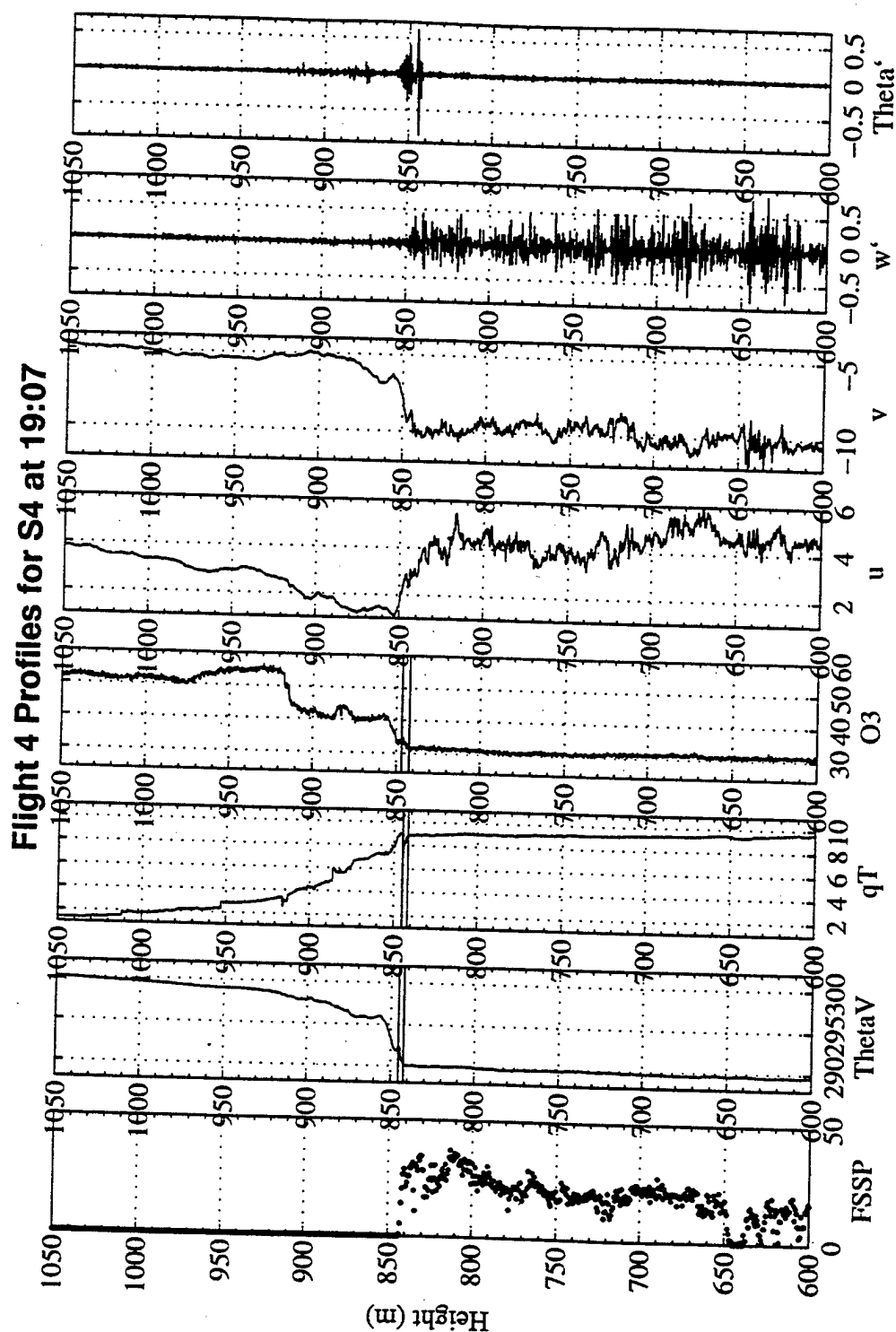


Figure 7 Example of Profiles and the Inversion Layer. Profiles of scalar quantities are shown as (a) cloud droplet concentration (N/cm³), (b) virtual potential temperature (K), (c) total water (g/kg), (d) ozone (ppbv), (e) u wind speed component (m/s), (f) v wind speed component, (g) wavelet decomposition of vertical velocity (m/s), and (h) wavelet decomposition of potential temperature

Corresponding jumps for each sounding in Flight 4 are given in columns 2-4 of Table 2.

Table 2 Properties of the Inversion Layers from Flight 4 Soundings. Columns 2-4 are the inversion jumps for total water (g/kg), ozone (ppbv), and virtual potential temperature (K), respectively. A positive jump indicates an increasing value with height. Column 5 is the depth of the inversion layer in meters. Column 6 is the virtual potential temperature gradient in the inversion layer (K/m). Column 7 is the cloud top height in meters.

Sounding	Δq_r	ΔO_3	$\Delta \theta_v$	Δz	$\nabla \theta_v$	Cloud-Top Height
S1	-0.5	-2.8	1.1	3.0	0.36	780.0
S2	-0.9	-3.9	2.1	1.8	1.18	805.0
S3	-0.8	-2.4	2.2	2.2	0.98	872.0
S4	-1.2	2.1	2.1	3.6	0.59	842.0
S5	-1.5	4.5	2.3	4.5	0.50	834.0
S6	-1.2	6.0	2.5	2.0	1.24	968.0
S7	-1.4	-2.7	2.6	3.2	0.81	819.0
S8	-1.5	-5.7	2.9	4.7	0.62	788.0
S9	-0.7	-2.7	1.4	2.2	0.64	814.0
S10	-0.5	1.0	0.3	1.6	0.19	734.0
S11	-1.1	4.4	2.0	2.2	0.88	913.0

An interesting outcome from the sounding profiles is the small depths of the inversion layers (column 5 of Table 2). The average depth of the layer was 2.8 meters for Flight 4. Similar mean depths were found for other flights. The increase in virtual potential temperature in this small layer is rather significant and results in an extremely strong temperature gradient. The gradient is substantially larger compared to a clear convective boundary layer (e.g., Deardorff, 1979)

The effect of such a strong inversion layer on an entraining updraft is analyzed using a parcel theory. Neglecting horizontal inhomogeneity, virtual effects, and mixing between the parcel and the environment, the vertical equation of motion following a parcel can be written as,

$$\frac{dw}{dz} = -\frac{g}{\Theta}(\Theta - \Theta_i), \quad (2)$$

where Θ and Θ_i are the potential temperatures of the penetrating parcel and the inversion layer, respectively. Assuming the parcel has the mean properties of its origin, (2) can be rewritten as,

$$w \frac{\partial w}{\partial z} = -\frac{g}{\bar{\Theta}}(\bar{\Theta} - \Theta_i), \quad (3)$$

where $\bar{\Theta}$ is the mean potential temperature of the cloud mixed layer. Integration of (3) from the base of the inversion, where $z=z_1$ and $w=w_0$, to the level where vertical velocity becomes zero ($z=z_u$ and $w=0$), yields,

$$\frac{1}{2} w_0^2 = \frac{\Delta\Theta (z_u - z_1) \cdot g}{\bar{\Theta}} = \frac{\Delta\Theta}{\Delta z} \frac{g}{\bar{\Theta}} (\Delta z)^2. \quad (4)$$

The maximum distance the parcel can penetrate is therefore given by,

$$\Delta z = \left(\frac{\bar{\theta}}{2g \Delta \theta} \right)^{\frac{1}{2}} w_0. \quad (5)$$

With a rather strong updraft (say, $w_0=1$ m/s), the weakest temperature gradient from Table 2 (S10 with a potential temperature gradient of .19 K/m), and a mean potential temperature of 290K, the maximum distance the updraft can penetrate is 1.7 meters. If the average updraft velocity is used ($\bar{w}_{up}=0.3$ m/s from Flight 4), the maximum distance the updraft can penetrate is only 0.5 meters. These estimates indicate that the majority of updraft parcels might not be able to penetrate through a very small layer at the base of the inversion. Since the average updraft cannot penetrate past this layer, it physically represents the limiting region in which direct exchange with the boundary layer will occur. The entrainment zone, where mixing between the boundary layer air and the air above occurs, thus can only be within this strong inversion layer. The inversion layer is therefore also the entrainment zone. Consequently, the changes in thermodynamic and scalar quantities across the inversion layer accurately describe the jump conditions in the entrainment zone.

An important aspect, however, of the definition of the entrainment zone is the impact of the definition on the jump conditions, which is also a difficult issue in the clear convective boundary layers. In other words, the value of the jump weighs heavily on the character or thickness of the entrainment zone, which varies between soundings. Inspection of the total water jump conditions from Table 2 reveals that the magnitude of the total water jump varies by

a factor of three, from -0.5 to -1.5. This is significant given that the jump conditions themselves are taken from a very small layer of only a few meters deep. It is also a vital concern, since the jump conditions are used in the calculation of entrainment velocity. An understanding of the source of variation in the jump conditions is therefore essential if the scope of the variability and its effect on entrainment is to be understood.

B. LAYERED STRUCTURE ABOVE THE ENTRAINMENT ZONE

A striking feature between the soundings analyzed for each flight is the layered structure above the entrainment zone. Sounding profiles, for example, typically show a layer 20-130 meters thick, which resides directly above the entrainment zone. This layer often contains strong perturbations in all variables, with intermittent turbulence within the layer. The mean of the variables, however, remains very well mixed. Signatures of cloud droplet concentrations are also observed in this layer at times, which suggests that this layer might have been part of a cloud layer at one time.

In addition to the layer immediately above the entrainment zone, other very apparent layers also appear at higher levels. These layers tend to possess fewer perturbations and, in fact, appear fairly well mixed at times, but with no signs of turbulence. The values of temperature, total water, and other scalars in these layers are generally between the boundary layer values and the respective values at several hundred meters above the

boundary layer, which suggests that they are possibly a mixture of boundary layer and free troposphere air properties. Consequently, the presence of these layers is possibly tied to boundary layer processes.

An example of an observed layered structure is depicted in Figure 8. This particular sounding shows a well-mixed boundary layer up to 1020 meters. Above the entrainment zone, a layer is identifiable up to 1040 meters, at which a weak inversion and a relatively sharp decrease in water vapor can be identified. The layer also shows strong vertical perturbations of total water, virtual potential temperature, and ozone. The wavelet analysis for vertical velocity and potential temperature show significant perturbations in the small scales within the layer, suggesting the presence of turbulence. In addition, the FSSP cloud droplet concentrations also indicate that some residual cloud droplets exist in the lower part of the layer. Above this first layer, a second layer also exists from 1040 to 1060 meters, a third from 1060 to 1100 meters, and a fourth layer resides from 1100 to 1130 meters. The profile of ozone yields a clear picture regarding the vertical variations in these upper layers. Clearly, the scalars distribute rather uniformly within each layer as if they were part of a mixed layer. A presence of turbulence, however, is not depicted in the wavelet analysis of vertical velocity for the upper layers.

The resounding presence of these observed layers above the entrainment zone is a viable concern in the study of entrainment. Since the structure of each layer, or most importantly the lowest layer, determines the magnitude of the gradient and depth of the entrainment zone, the presence of these layers therefore determines the jump conditions

Flight 7 Profiles for S1 at 17:41

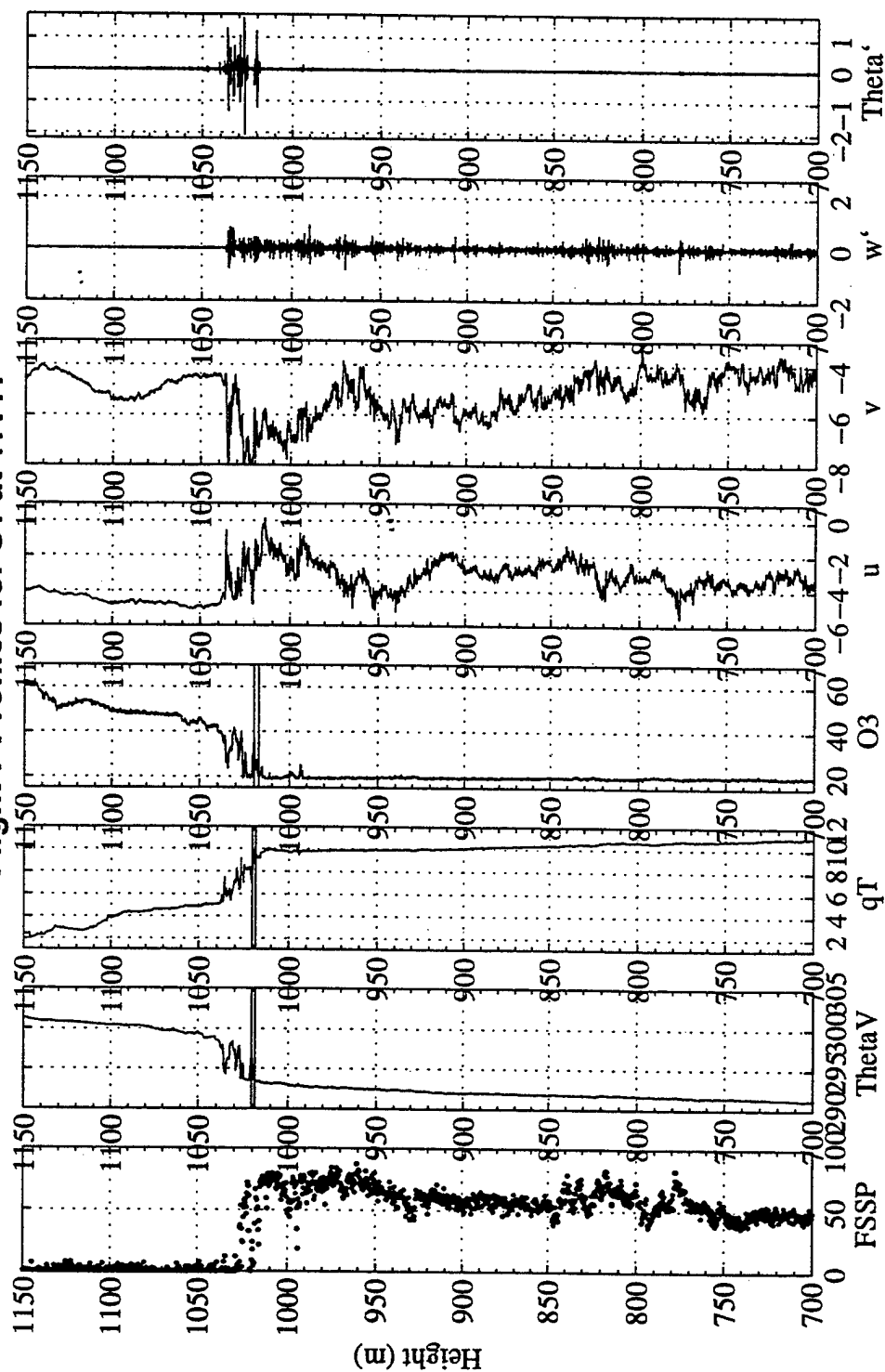


Figure 8 Depiction of Layered Structure Above the Entrainment Zone. Profiles are the same as those given in Figure 7.

used in the calculation of entrainment velocity. The physical existence of the layers thus adds a level of complexity to determination of the entrainment rate. As a result, it is imperative to understand the formation of the layered structure above the entrainment zone.

C. HYPOTHESIS ON FORMATION OF LAYERED STRUCTURE

An initial understanding of the formation of layers above the entrainment zone comes about by comparing the variation in the cloud top height with the vertical range of the layered structure. Table 2 (Column 7) shows that the boundary layer height varies between 730 m and 970 m. The range of this variation correlates remarkably well with some of the layers that exist above the entrainment zone for Flight 4, suggesting that these layers were probably part of the boundary layer in its history. Similar observations are also obtained from other flights. From this observation and the properties of the layers discussed earlier, some possibilities that may lead to the formation of these layers are now discussed.

1. Entrainment Drying

One approach towards understanding the development of the structured layer above the entrainment zone is to consider the presence of layers as a history of the local cloud top evolution. Now consider the changes to the structure of the upper boundary layer that could occur if the local cloud top height begins to decrease as a result of

entrainment drying in the upper portion of the cloud layer. This scenario could happen if the time scale of boundary layer mixing is large compared to that of the entrainment mixing. This would satisfy the condition that there be sufficient dry inversion air to mix with the upper cloud layer to cause the cloud to dissipate. Therefore, as sufficient dry air is drawn into the cloud layer, the cloud droplets are evaporated, resulting in a total or partial decrease in droplet concentration within a finite volume of the upper cloud layer. Consequently, the source of TKE also decreases as the cloud dissipates. Mixing of the layer, however, continues before the turbulence completely dissipates. Any residual turbulence may then cause entrainment mixing with the previous entrainment zone. The gradients of all scalars in the previous inversion decrease due to entrainment mixing by the residual turbulence as a result. In addition, as the cloud dissipates, the gradient of potential temperature also decreases at the previous inversion level since there is no more radiative cooling to maintain the inversion.

Meanwhile, radiative cooling at the newly formed cloud top generates turbulence mixing in the remaining boundary layer while a new inversion forms at the new cloud top due to radiative cooling and the subsequent turbulent mixing in the boundary layer. As the boundary layer moistens from mixing with the near-surface air, a gradient in total water also forms at the new inversion. The drying process described above is illustrated in the conceptual sketch in Figure 9(a). The lowest layer formed from this process will be further referred to as the first residual layer.

The description given for the entrainment drying effect is substantiated by many of the FIRE profiles, whereby the

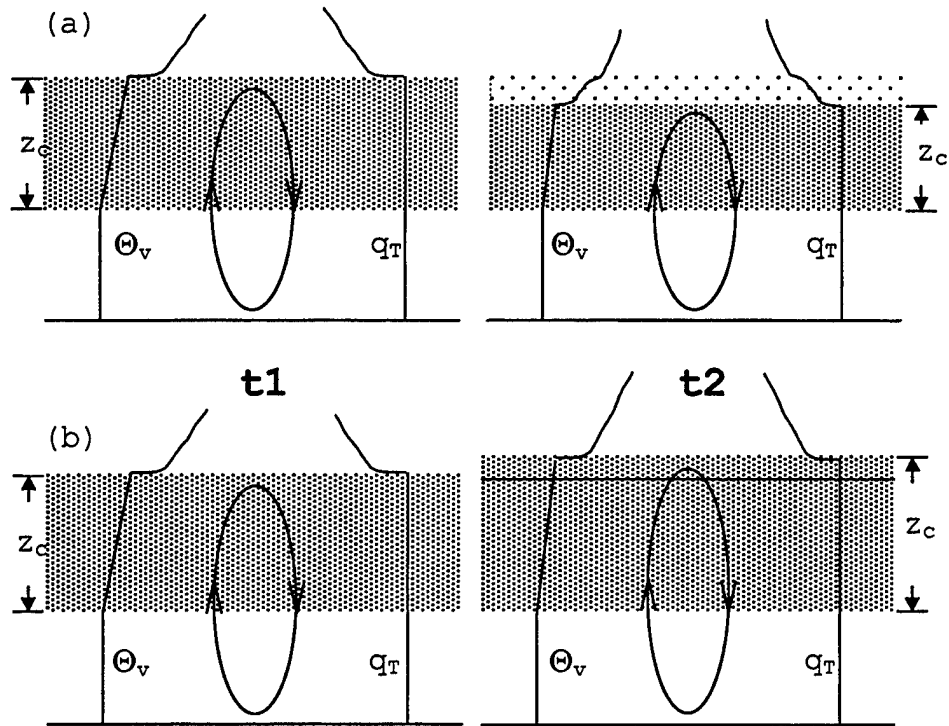


Figure 9 Idealized Schematic of the Entrainment Drying Effect. Stages of cloud top evolution for two hypothetical times t_1 and t_2 are depicted in (a) for the decreasing cloud top and in (b) for the growing cloud top. Vertical profiles refer to those of virtual potential temperature and total water. z_c indicates the cloud depth. The circulation between the profiles suggests a boundary layer circulation.

history of past cloud layers is very apparent. One such example is shown in Figure 10. Here, the layers above 875 meters are non-turbulent. The layers are, however, vertically homogeneous. This suggests that these layers were at one time fully turbulent and well mixed. The time period for the residual turbulence to persist can be estimated using the dissipation rate of turbulence kinetic

energy (TKE) described by,

$$\frac{\partial e}{\partial t} = -\varepsilon, \quad (6)$$

where e is TKE and ε is the dissipation rate. The expected time for complete dissipation of the turbulence can then be determined using,

$$t = \frac{e}{\varepsilon}. \quad (7)$$

Assuming $e \approx 0.30 \text{ m}^2/\text{s}^2$ and $\varepsilon \approx 0.0001 \text{ m/s}^3$, the turbulence is expected to dissipate fully in 3000 seconds, or in less than an hour. This implies that the residual layers, which are not turbulent, have existed for more than an hour. This is certainly true for the layers above 875 meters in Figure 10. For the layer between 830 and 875 meters, however, some residual turbulence is apparent. Examination of the wavelet analysis of potential temperature shows that mixing is still occurring in this layer. The downward evolution of the cloud top is therefore explained by the presence of non-turbulent layers over layers containing turbulence and residual mixing.

Another indication of the history of the local cloud top is also found in Figure 10 between the entrainment zone and 830 meters. Here, a strong turbulent layer exists with an indication of a past jump condition at 830 meters and the formation of a new jump below the entrainment zone. Significant vertical variations in the conserved variables are also evident in this layer, which reflects the recent formation of the layer. This strengthens the hypothesis that the downward formation of layers is occurring as entrainment drying reduces the cloud droplet concentrations in discrete jumps.

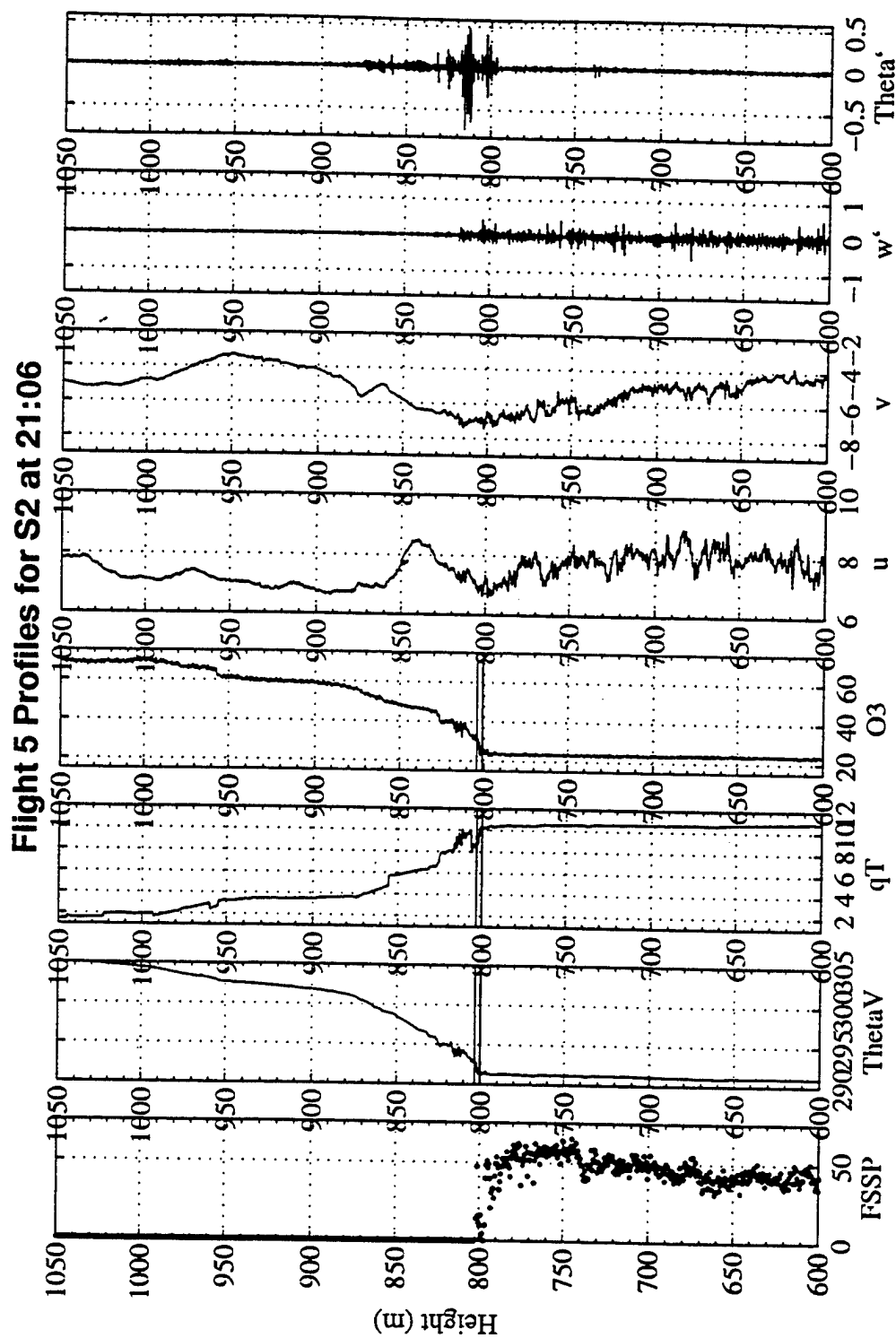


Figure 10 Depiction of History of the Cloud Top. Profiles are the same as those given in Figure 7 and 8.

An example of a composite time sequence depiction of the entrainment drying effect is shown in Figure 11 and Figure 12. These two soundings, S7 and S8 from Flight 4 respectively, depict the downward progression of the formation of the residual layers as the upper stratocumulus cloud dissipates. Figure 11 shows at least two very distinct layers above the mixed layer. The first residual layer, from 820 to 840 meters, contains strong vertical variations in the scalar variables. The wavelet depiction of turbulence reflects mixing in the layer, but the turbulence is weak compared to the boundary layer below as seen in the profile of vertical velocity perturbations. Some cloud droplets also remain in the layer. The inversion and the jumps in total water and ozone are still rather significant and the location of the inversion still corresponds to the top of the remaining cloud droplets. From 840 to 875 meters, a second layer exists, which is topped by another weak inversion at about 875 m and corresponding rapid changes in water vapor and ozone. This weak inversion layer is likely the height of the cloud top before the one at 840 m formed. No cloud droplets exist in this second residual layer and the turbulence is extremely weak. Meanwhile, at 820m, a new inversion is under development at the newly formed cloud top. The change in water vapor appears to be more significant than in temperature and ozone.

The next stage of the layered development is shown by another sounding (S8) made about 20 minutes later. Since the sounding was not made in exactly the same location as S7, the height of cloud top and the first residual layer is not exactly the same. Again, the first residual layer is

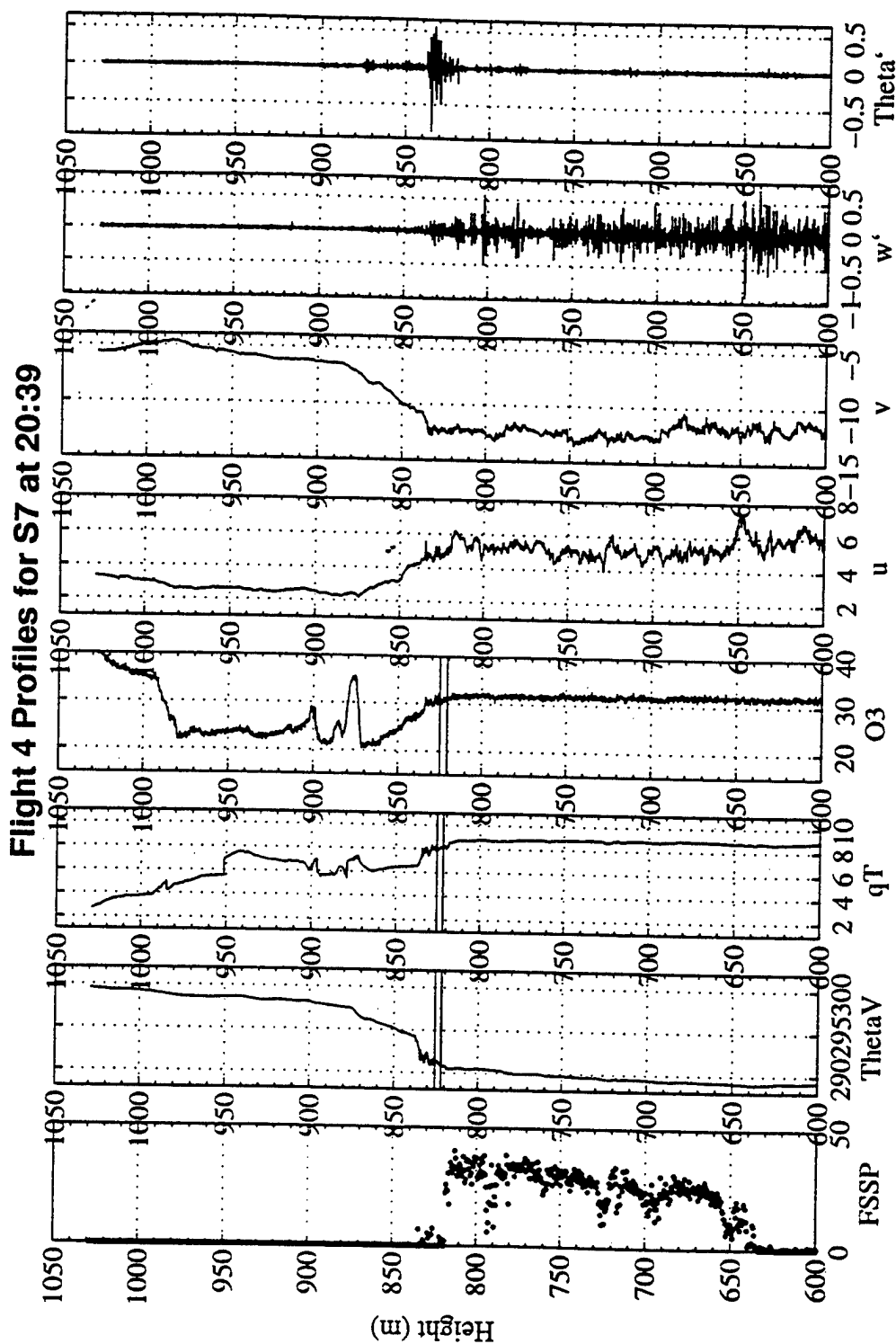


Figure 11 Example of Time Sequence Depiction of Entrainment Drying Effect
 Profiles are the same as those given in Figure 7 and 8.

weakly turbulent, but appears weak compared to that in S7. In the lower layer, now from 790 to 835 meters, the cloud droplets have evaporated from S7, and turbulence has decreased. The jump condition of the conserved variables has consequently increased in the newly shaped entrainment zone, as radiative cooling at the cloud-top is enhanced by the lack of lingering cloud droplets above the main stratocumulus cloud deck.

It should be mentioned that the layered structure above the cloud top only depicts the lowering of the cloud-top height through entrainment drying. Growth of the local cloud top height, as illustrated in the lower panel of Figure 9, cannot be identified from soundings at an earlier time. Such growth would occur in cases of strong boundary layer turbulence mixing, where the entrained dry air is quickly mixed with a large volume of cloud and boundary layer air. Because of the strong horizontal variability of turbulence mixing in the boundary layer, it is likely that both growth and lowering can occur locally but at different locations. Therefore, the lowering of the cloud top height observed from the soundings is not necessarily indicative of a decrease of an ensemble cloud top heights for a general area. Nevertheless, if the boundary layer turbulence mixing is decreased, as a result of decoupling during daytime for example, it is possible that the ensemble boundary layer height lowers as a result of entrainment drying.

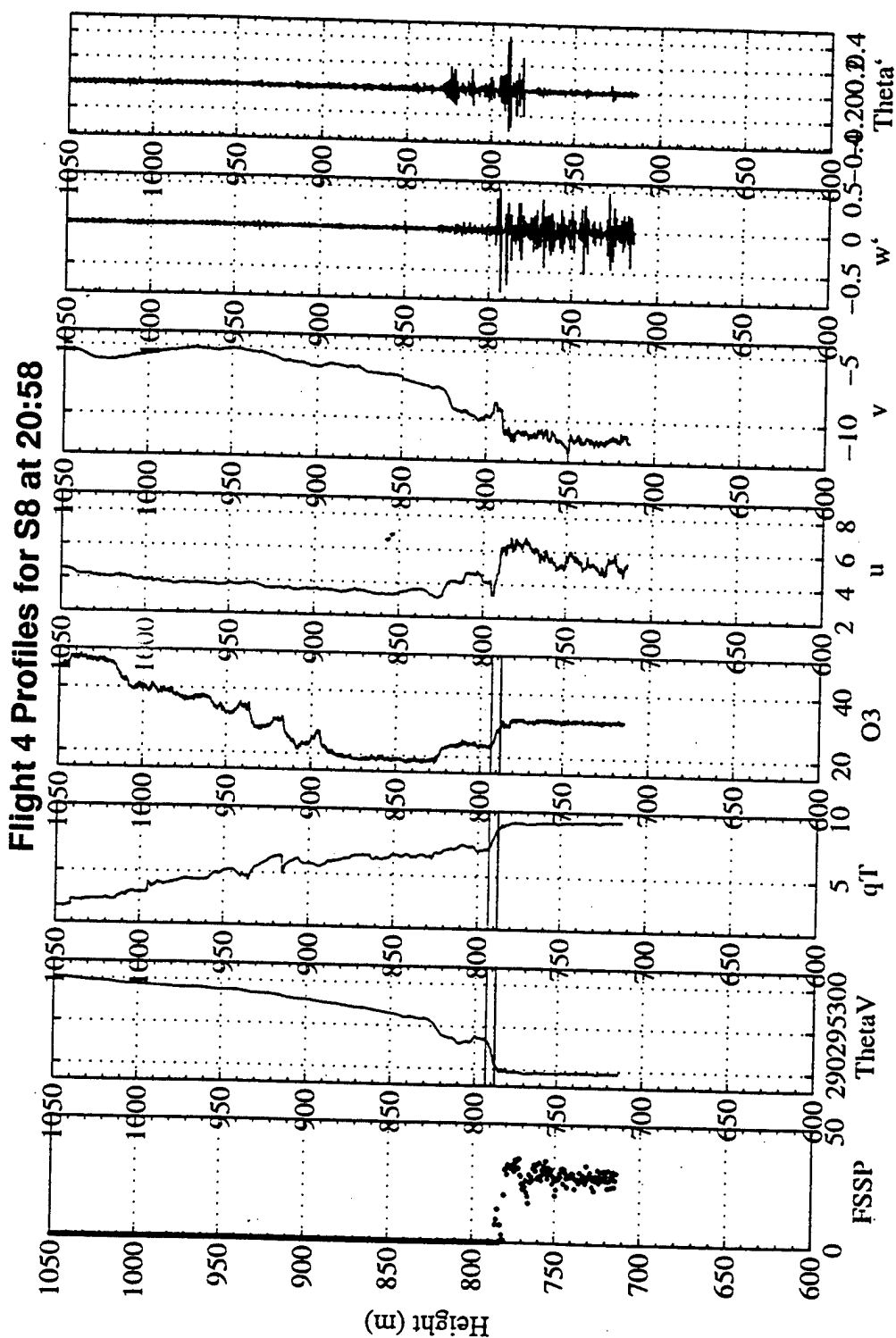


Figure 12 Example of Time Sequence Depiction of Entrainment Drying Effect
 Profiles are the same as those given in Figure 7 and 8.

2. Other Possibilities

A detail that is not explained well by the entrainment drying hypothesis is found when the residual layers above the entrainment zone do not possess a mixture consistent with the boundary layer and above boundary layer ozone structure. Ozone is specifically mentioned because this inconsistency seems to only occur in the ozone profiles. An example of this situation is found in Figure 12, where the above ozone structure consists of a high ozone concentration of 40 ppbv whereas the boundary layer ozone is well mixed at approximately 32 ppbv. In the residual layers above the entrainment zone, however, layered ozone concentrations of 20-25 ppbv are found. This variation therefore appears to be inconsistent with the idea that the residual layers are a mixture of the above boundary layer and cloud mixed-layer ozone.

One possible cause of the observed inconsistency in the ozone residual layer structure is horizontal advection through a depth corresponding to the range of depths of observed layers. Lenschow et al. (1980) suggested that ozone is commonly inhomogeneous above the boundary layer. It therefore seems reasonable that the advection of higher or lower values of ozone could be occurring and complicating the residual layer structure.

Layers of prominent ozone and/or water vapor anomalies from above the subsidence inversion were studied for some of the FIRE measurements by Kloesel (1993). Kloesel (1993) suggests that these layers were the result of an intrusion of air from the middle and upper troposphere. The layers studied by Kloesel (1993) are different from the layers identified here. The layers from this study are closer to

the boundary layer top and the differences between layers are less prominent than those studied by Kloesel. Evidently, these layers are associated with the boundary layer processes rather than synoptic perturbations. However, the possibility that the layers studied by Kloesel (1993) may extend down to the immediate top of the entrainment zone cannot be excluded. The influence of these layers may be the reason that entrainment drying cannot account for some of the observed layer structure from the soundings.

V. ENTRAINMENT VELOCITY

A. ENTRAINMENT VELOCITY VARIABILITY

The variability of entrainment zone jump conditions between different soundings from one flight is seen in Chapter IV Table 2. Clearly, each sounding results in very different entrainment rates using Equation (1), as depicted now in Table 3. The entrainment rate varies by a factor of three between soundings. Since the entrainment flux used in the calculation was kept the same, the variability shown in Table 3 reflects that in the jump conditions.

The large variability in the entrainment rate estimated for one flight for individual soundings indicates that a single sounding cannot be used to obtain the properties of the entrainment zone and entrainment jump conditions. As discussed in Chapter II, the jump condition required for the entrainment rate calculation is defined by the change of the quantity across the entrainment zone (Figure 3), which has a depth of about 25% of the depth of the clear convective boundary layer. The outermost extent of the entrainment zone is determined by the level penetrated by the strongest updrafts at any given time. Since updraft parcels with different vertical velocities may penetrate differently into the free troposphere, a particular sounding may chance to pass through the vicinity of an active updraft, whereby a deeper upper limit of the entrainment zone would result. As pointed out in Deardorff (1980), however, only an average of several (or many) soundings can give reliable estimates of the thickness of the entrainment zone and the properties at its lower and upper edges. Consequently, the

top of the entrainment zone should be determined as an ensemble average of the outermost penetration shown in each sounding. Similarly, the base of the entrainment zone is the average boundary layer top over all soundings. The jump condition of a particular scalar quantity is therefore the mean jump condition from all soundings.

Based on this discussion, a mean jump condition was obtained for each flight by averaging the jump conditions obtained from all the available soundings. The resultant mean jumps in total water and ozone and the corresponding entrainment rate is given in Table 4 for all nine flights during FIRE. These entrainment rates from total water are generally in the range between 0.8-4.7 cm/s. Negative entrainment rates were obtained from Flights 4, 5, 6, and 8, which are obviously unrealistic. The ozone fluxes from these flights are not consistent with the sign of the mean jump condition. Table 3 also shows large variations in the ozone jump across the entrainment zone, which seems to indicate strong ozone variation on a scale larger than the 60 km covered by one flux measurement leg. These results certainly raise concerns with using ozone for entrainment rate estimates even though it is a conserved variable. More study should be done to examine the representation of ozone flux from a limited area such as that covered by a regular measurement leg of usually less than 100 km.

Table 3 Entrainment Velocity Using Total Water Jump Conditions. Values are given in cm/s for each sounding using equation (1) in Chapter II.

Sounding	W_e
S1	2.7
S2	1.5
S3	1.7
S4	1.1
S5	0.9
S6	1.1
S7	1.0
S8	0.9
S9	1.9
S10	2.7
S11	1.2

Table 4 Entrainment Velocities for each FIRE Flight Using Mean Jump Conditions. Entrainment velocities for total water and ozone are given in columns 3 and 5 in cm/s. Average jump conditions for each flight are given in columns 2 and 4. A positive jump condition indicates an increase in height.

Flight	Mean Δq_T	We (q_T)	Mean ΔO_3	We (O_3)
2	-.57	2.0	3.22	0.3
3	-.73	3.2	2.72	3.7
4	-1.02	1.3	-0.18	-16.7
5	-1.38	1.3	6.48	-0.6
6	-.36	0.9	1.40	-0.7
7	-.71	0.8	3.80	0.5
8	-.85	1.5	2.43	-0.4
9	-.11	4.7	17.19	1.2
10	-.56	3.0	4.73	0.6

B. AN ALTERNATIVE METHOD FOR CALCULATING ENTRAINMENT VELOCITY

A major problem associated with the entrainment rate calculation discussed in the previous section is the statistical representativeness of the soundings used to obtain the ensemble average jump conditions. Theoretically, the soundings should be at least one boundary layer height apart to ensure independence between each sounding. This requirement is generally met with aircraft soundings. However, the number of soundings available for averaging is usually insufficient, resulting in large uncertainties even when calculating the entrainment rate using average jump conditions. In this section, an attempt is made to develop a modified averaging method for the jump conditions in hope for better ensemble representativeness. The results from the new method will be compared with those from the previous method.

The basic idea of the modified method is to consider time averaging as well as spatial averaging of the jump conditions to obtain a representative ensemble jump condition. A time averaging is desirable for the stratocumulus-topped boundary layer for two reasons. First, and as discussed in Chapter IV, the local mixing with the above boundary layer air is likely to occur in a small layer of several meters in depth above the boundary layer in cloudy conditions due to the extremely strong inversion. The region of entrainment is thus confined to a small layer following the interface between the cloud and the air above. Unlike the clear convective boundary layer, the interface between the cloud and the air above is also clearly defined

by the presence of the cloud layer, as seen in the sounding profiles shown in chapter II. The second reason for time averaging is that the depth of the stratocumulus-topped boundary layer varies slowly with time compared to a clear convective boundary layer, where entrainment may result in rapid growth of the boundary layer. The relative steady state of the boundary layer height in the cloudy case allows penetrations of updrafts of different vertical velocities at a particular local interface. Therefore, the depth of the entrainment zone from one sounding represents the effect of the strongest updrafts in the history of this interface. A particular updraft with intermediate vertical velocity thus entrains the integrated mixture of all previous updrafts of stronger vertical velocity.

Based on the above considerations, a time averaged jump condition can be derived using a single sounding in cloudy conditions by considering penetrations of updrafts with a spectrum of updraft velocities. Given a temperature gradient of the inversion layer from the sounding, a simple parcel model can be used by first considering the penetration of an updraft as it moves into the inversion layer. As the parcel moves into the layer, it loses kinetic energy and gains potential energy as it overcomes the negative buoyancy force. Consequently, the distance it can travel within the entrainment zone is dependent on the updraft's TKE before it enters the inversion layer and on the strength of the stability in the layer, which is described in Equation 5. Equation 5 can be rewritten as,

$$\Delta z = \left(\frac{\overline{\theta}}{2g\gamma} \right)^{\frac{1}{2}} w_o, \quad (8)$$

where γ is the gradient of potential temperature, w_0 is the velocity of the updraft, $\bar{\theta}$ is the mean boundary layer potential temperature, and g is gravity. If a linear gradient of a conserved scalar ϕ is assumed through a finite depth Δz , then the jump experienced by the scalar and an individual updraft, j , can be expressed as,

$$\Delta\phi_j = \int_{z_i}^{z_i+\Delta z_j} \frac{\partial\phi}{\partial z} dz = \Gamma_{\phi} \cdot \Delta z_j, \quad (9)$$

where z_i is the height of the base of the inversion. Substituting (8) into (9),

$$\Delta\phi_j = \Gamma_{\phi} \left(\frac{\bar{\theta}}{2g\gamma} \right)^{\frac{1}{2}} w_j, \quad (10)$$

gives the jump condition experienced by an individual updraft with velocity w_j as it penetrates a layer with a gradient of $\Gamma_{\phi j}$. If the contribution of all updrafts is considered, then an updraft ensemble jump condition can be written as,

$$\overline{\Delta\phi} = \int_{-\infty}^{+\infty} p_{\Delta\phi} \cdot \Delta\phi \cdot d\Delta\phi, \quad (11)$$

which describes the mean jump condition experienced by an ensemble of updrafts. Here, $p_{\Delta\phi}(\Delta\phi)$ refers to the probability density function of $\Delta\phi$. Substituting $\Delta\phi$ from (10) into (11), we obtain,

$$\overline{\Delta\phi} = \int_{-\infty}^{+\infty} p_{\Delta\phi} \cdot \Gamma_{\phi} \cdot \left(\frac{\bar{\theta}}{2g\gamma} \right)^{\frac{1}{2}} \cdot w \cdot d\Delta\phi, \quad (12)$$

If the probability density function for vertical velocity is $p_w(w)$, then,

$$p_{\Delta\phi} \cdot d\Delta\phi = p_w \cdot dw. \quad (13)$$

Substituting (13) into (12) yields,

$$\overline{\Delta\phi} = \int_{-\infty}^{+\infty} \Gamma_r \cdot p_w \cdot w \cdot dw = \Gamma_r \cdot A \cdot \overline{w_o}, \quad (14)$$

where $\overline{w_o}$ the average updraft velocity in the mixed layer and A is defined from (10) as,

$$A = \left(\frac{\overline{\Theta}}{2g\gamma} \right)^{\frac{1}{2}}. \quad (15)$$

Equation (14) thus gives the time averaged jump condition at the location of the sounding. Since this approach uses the gradients of potential temperature and the scalar, this method is further referred to as the gradient method.

Examples of the time averaged jump in total water and ozone are shown in Figures 13 and 14. In these plots, the jump conditions used in the original calculation of the entrainment velocity (referred to as the maximum jump conditions) are compared to the time-averaged jump conditions from the gradient method. Both figures clearly show that the magnitudes of the time-averaged jump conditions vary at a small fraction of the variation of the maximum jump condition from individual soundings. This is expected due to the averaging process that accounts for contributions from all updrafts. Such smaller variation among different soundings certainly reduces the random error associated with spatial averaging of all soundings to be performed before a new entrainment velocity is calculated.

Results from both examples also show that the mean jump from the gradient method is smaller than the maximum jump used in the previous entrainment rate calculation, which reflects the suppression of updrafts by the strong inversion. In the example of Flight 4 (Figure 14), it seems

that the averaged jump is still correlated with the maximum jump when the maximum jump has a small magnitude (a result of either a thin inversion or a small gradient). In the case of a substantial maximum jump, the time-averaged jumps from different soundings are nearly independent of the maximum jumps.

The calculation of entrainment velocity can now be performed using the jump conditions from the gradient method in Equation (1). The results for all nine FIRE flights are shown in Table 5. The entrainment fluxes used in the calculation were given in Table 2. Ensemble jump conditions used in the calculation consisted of an average of all time-averaged jumps for each flight. These values are suggested to represent the space and time average of updrafts penetrating into the entrainment zone. It is noted that the new method does not eliminate the unrealistic entrainment velocities from the ozone flux on Flights 5, 6, and 8, however.

Table 5 Entrainment Velocities for each FIRE Flight Using the Gradient Method. Entrainment velocities for total water and ozone are given in columns 3 and 5 in cm/s. The ensemble jump conditions across the entrainment zone and used in the calculation for entrainment velocity are given in columns 2 and 4. A positive jump condition indicates an increase in height.

Flight	Mean $\overline{\Delta q_T}$	We (q_T)	Mean $\overline{\Delta O_3}$	We (O_3)
2	-.26	4.4	1.30	0.8
3	-.38	6.2	1.30	7.7
4	-.52	2.6	0.03	1.0
5	-.54	3.4	2.49	-1.6
6	-.24	1.3	0.69	-1.4
7	-.48	1.1	2.64	0.8
8	-.33	3.9	0.54	-1.9
9	-.03	17.3	2.70	7.4
10	-.22	7.7	1.17	2.6

Gradient Method Comparison for Flight 2

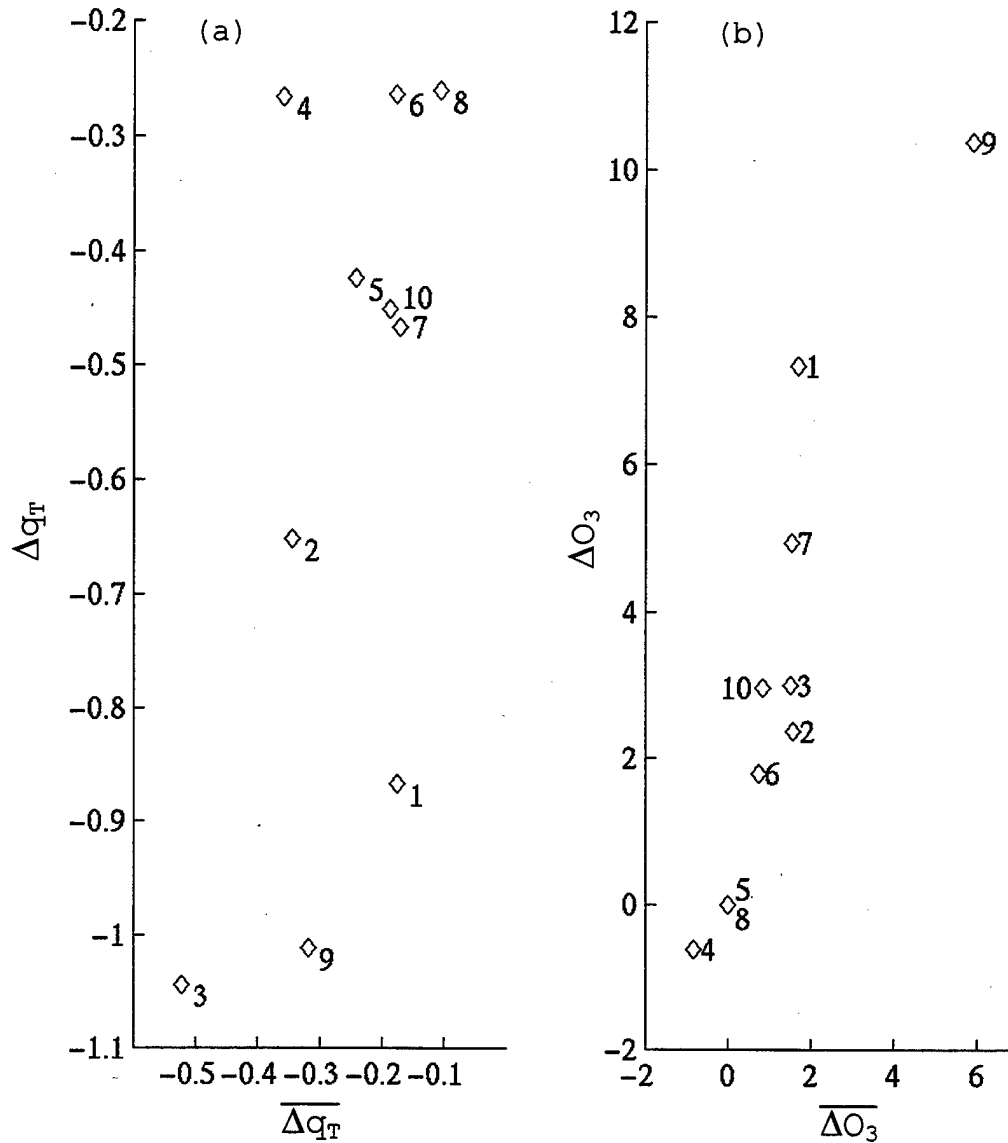


Figure 13 Comparison Between Maximum Jump Conditions and the Time-Averaged Jump Conditions for Flight 2. Maximum jump conditions are plotted on the y-axis for (a) total water and (b) ozone. Time-averaged jump conditions determined using the gradient method are plotted on the respective x-axis.

Gradient Method Comparison for Flight 4

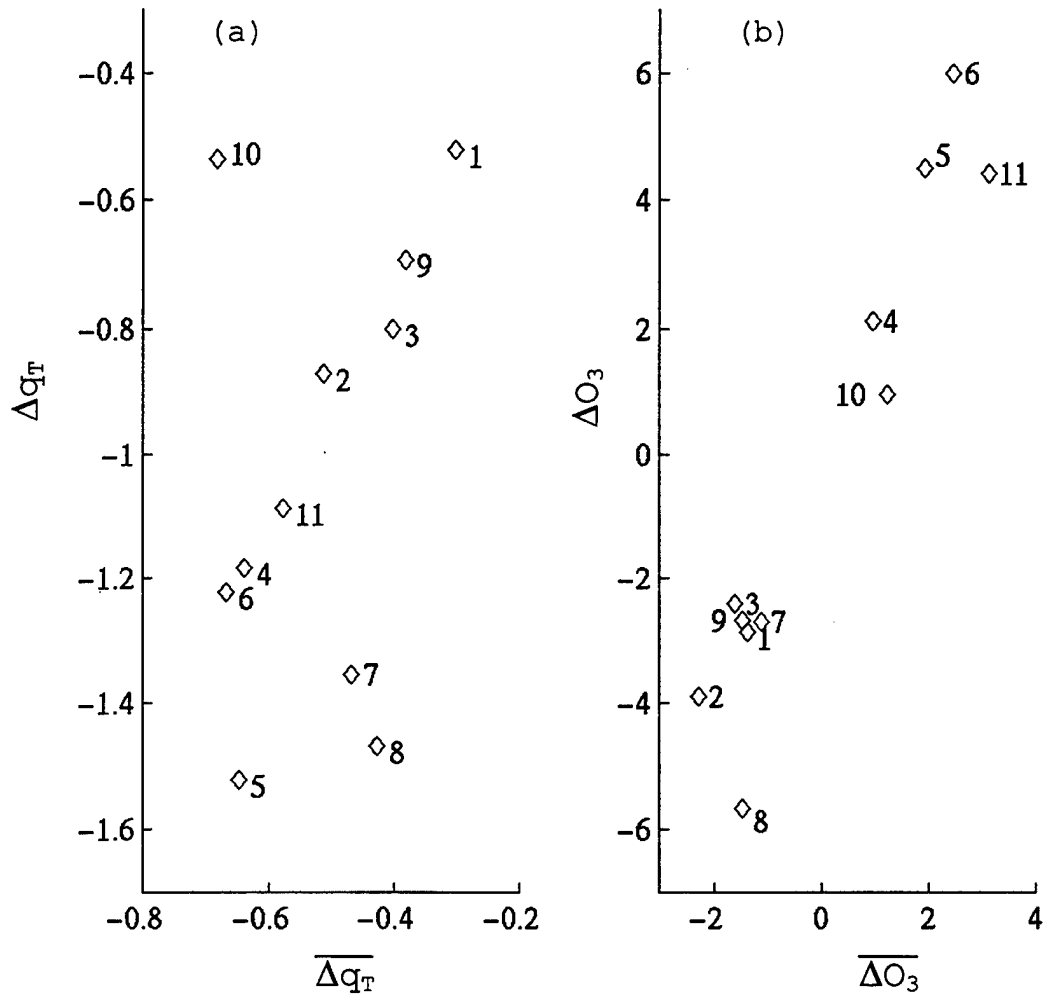


Figure 14 Same as in Figure 16, except for Flight 4.

VI. SUMMARY, CONCLUSIONS, AND DISCUSSIONS

A. SUMMARY AND CONCLUSIONS

The overall objective of this thesis was to understand the properties of the entrainment zone and to explore a new method of determining entrainment rate for the stratocumulus-topped boundary layer. Aircraft soundings and horizontal measurements by the NCAR Electra during FIRE were used for this analysis. The analysis was based on measurements from all nine flights, although most of the examples shown are from Flight 4. Entrainment fluxes and entrainment rates are given for all the flights.

The entrainment fluxes were obtained by linear extrapolation of the observed flux profiles in the cloud mixed layer to the cloud top height. The average cloud-top height, or equivalently, the boundary layer top, was obtained from the downward lidar measurements or from sounding profiles when lidar measurements were not available.

An in-depth analysis of the inversion structure from the sounding profiles revealed the unique inversion structure at the stratocumulus top. The inversion layer is extremely shallow, usually less than 10 m, but with strong temperature inversion as well as large changes in other scalars and sometimes in the mean horizontal wind components. Using a simple parcel theory and measurements from Flight 4, it is estimated that the maximum penetration of a typical updraft parcel is less than 2 meters. As a result, the entrainment zone was defined as the lowest

strong gradient layer of only a few meters deep, which existed directly above the mixed layer. The jump conditions used for the initial estimate for entrainment velocity therefore consisted of the change in conserved variables through this zone.

An important aspect of the determination of the jump conditions for the entrainment zone was the variability found in the jump conditions themselves. For Flight 4, jump conditions between individual soundings varied by a factor of three. This was an important concern, since the jump conditions are used in the calculation of entrainment velocity. Variation in the jump conditions was shown to lead to variation in the entrainment rate, and therefore an unrealistic representation of boundary layer dynamics. The source of jump condition variability was thus analyzed in order to understand the variation and the scope of the variability on entrainment.

Layered structure above the entrainment zone was found to be a common feature between soundings. These layers were typically 20-130 meters thick and resided immediately above the cloud mixed layer. The lowest layer was found to have weak or intermittent turbulence, whereas the uppermost layers were non-turbulent, but scalar variables conserved in adiabatic mixing processes were vertically homogeneous. This suggested that the upper layers were at one time turbulent and that the turbulence had dissipated. An estimate of the time needed to fully dissipate the turbulence without a source of TKE suggests a time scale of less than an hour. Therefore, for those soundings where turbulence was identified in the first residual layer, the layer may have been formed within an hour of the measured sounding. A calculation regarding the expected dissipation

rate of turbulence confirmed that still fully turbulent layers, or those possessing residual turbulence, were formed within an hour of the measured sounding. The formation of the layers was therefore determined to be the result of boundary layer processes and a reflection of the history of cloud top evolution.

The formation of the layered structure about the local cloud top was considered the result of entrainment drying as illustrated in the upper panel of Figure 9. In this theory, entrainment was considered to evaporate cloud droplets within a finite depth of the cloud layer. As the cloud droplets evaporate, the cloud height decreases and a new layer is formed as any residual turbulence dissipates. A new jump is created at the newly formed cloud top as radiative cooling acts to increase the gradient of virtual potential temperature. This then results in the formation of a new entrainment zone and corresponding new jump conditions.

To minimize the uncertainty due to variation of jump conditions in the entrainment zone, a gradient method for calculating entrainment velocity was presented. In this approach, a new jump condition based on the penetration of an ensemble of updrafts through a layer with a given virtual potential temperature gradient in a single sounding was developed. This is based on the assumption that the stratocumulus-topped boundary layer height varies slowly compared to the time scale of boundary layer large eddy circulation so that updrafts of various vertical velocities may attempt to penetrate through the same cloud top. The jump across the inversion layer thus only represents the effect of the strongest updraft, while the mean difference between air property entrained by the updrafts and the

boundary layer air should be weighted by the probability distribution of updraft vertical velocity. An average jump condition can thus be derived based on one sounding that represents the time-average of the jump conditions at a local cloud top. The ensemble jump condition used to calculate the entrainment rate is further obtained by averaging over all soundings at different locations. This method of estimating the jump condition is physically based and showed less variation (by a factor of two) from sounding to sounding. The small variation among soundings certainly reduces the requirement on the number of soundings that should be used to obtain a statistically sound ensemble mean of the jump conditions and thus increases our confidence in the entrainment velocity estimate using the new jump conditions. The new entrainment rate for all FIRE flights were shown in Table 5.

B. DISCUSSION

The new gradient method for obtaining an ensemble jump condition offers an appealing improvement for determining an entrainment velocity that accurately reflects the boundary layer dynamics using a limited number of soundings. However, the inconsistency between entrainment velocity estimated with different scalar quantities (Table 5) suggests room for improvement. One such improvement is in increasing the number of soundings used for jump condition estimates, which relies on measurement design and flight planning in future field experiments. Another aspect, which has not been discussed in this thesis, is in the improvement of entrainment flux estimates. Ozone flux, in particular,

needs to be quantified to better accuracy given its large spatial variability as seen from the soundings. The 60 km horizontal leg used for ozone flux calculations is determined insufficient to represent the variation of fluxes in a larger area, resulting in unrealistic entrainment estimates. This was found to be true for FIRE Flights 5, 6, and 8.

The layer structure above the entrainment zone may have significant impact on the dynamics of entrainment process at the interface. In their tank experiment on the entrainment process in a clear boundary layer, Deardorff (1980) found that the entrainment rate was very different when the entrainment zone was capped by a neutral layer rather than a stable layer. Kantha et al. (1977) and Linden (1975) also found similar effects of a two-layered structure in the ocean mixed layer. Up to now, the effect of the neutral residual layers ($\partial\theta/\partial z \approx 0$) has not been studied for the stratocumulus-topped boundary layers and should be a subject of future investigation. A quantitative understanding of the process of entrainment drying would enable prediction of the entrainment zone properties and the associated jump conditions.

The parcel theory used in the gradient method is an initial attempt for improved ensemble averaging of the jump conditions. Measurements from tank experiments for the convective boundary layer (Deardorff, 1979) indicated discrepancies in the depth of the entrainment zone when the parcel theory is used, particularly in case of large Richardson numbers. Nevertheless, the time-averaged jump condition indeed shows less variability compared to the

maximum jump from each sounding, suggesting the validity of the averaging concept.

LIST OF REFERENCES

- Albrecht, B. A., R. S. Penc and W. H. Schubert, 1985: An observational study of cloud-topped mixed layers. *J. Atmos. Sci.*, **42**, 800-822.
- Albrecht, B. A., D. A. Randall and S. Nicholls, 1988: Observations of marine stratocumulus during FIRE. *Bull. Amer. Meteor. Soc.*, **69**, 618-626.
- Betts, A. K., and Boers, R., 1990: A cloudiness transition in a marine boundary layer. *J. Atmos. Sci.*, **47**, 1480-1497.
- Bolton, D., 1980: The computation of equivalent potential temperature. *Mon. Wea. Rev.*, **108**, 1046-1053.
- Brost, R. A., J. C. Wyngaard and D. H. Lenschow, 1982: Marine stratocumulus layers. Part: Turbulence budgets. *J. Atmos. Sci.*, **39**, 818-836.
- Buck, A. L., 1981: New equations for computing vapor pressure and enhancement factor. *J. Appl. Meteor.*, **20**, 1527-1532.
- Caughey, S. J., B. A. Crease, and W. T. Roach, 1982: A field study of nocturnal stratocumulus II Turbulence structure and entrainment. *Quart. J. R. Met. Soc.*, **108**, 125-144.
- Cox, S. K., D. McDougal, D. Randall, and R. Schiffler, 1987: FIRE- The first ISCCP Regional Experiment. *Bull. Amer. Meteor. Soc.*, **68**, 114-118.
- Deardorff, J. W., 1976: On the entrainment rate of a stratocumulus-topped mixed layer. *Quart. J. R. Met. Soc.*, **102**, 563-582.
- Deardorff, J. W., 1979: Prediction of convective mixed-layer entrainment for realistic capping inversion structure. *J. Atmos. Sci.*, **36**, 424-436.
- Deardorff, J. W., 1980: Cloud-top entrainment instability. *J. Atmos. Sci.*, **37**, 131-147.
- Garratt, J. R., 1992: *The Atmospheric Boundary*, Cambridge University Press.

Hignett, P., 1991: Observations of diurnal variation in a cloud-capped marine boundary layer. *J. Atmos. Sci.*, **48**, 1474-1482.

Kantha, L. H., O. W. Phillips, and R. S. Azad, 1977, On turbulent entrainment at a stable density interface. *J. Fluid Mech.*, **79**, 753-768.

Kloesel, K. A., B. A. Albrecht and D. P. Wylie, 1988: FIRE marine stratocumulus observations ---- summary of operations and synoptic conditions. FIRE Tech. Rep. NO.1, The Pennsylvania State University, Dept. of Meteorology, University Park.

Kloesel, K. A., 1993: Above-inversion profiles of moisture and ozone observed during FIRE. *Bull. Amer. Meteor. Soc.*, **121**, 683-694.

Latham, J., and R. L. Reed, 1977: Laboratory studies of the effect of mixing on the evolution of cloud droplet spectra. *Quart. J. R. Met. Soc.*, **103**, 297-306.

Lenschow, D. H., J. C. Wyngaard, and W. T. Penell, 1980: Mean Field and second-moment budgets in a baroclinic, convective boundary layer. *J. Atmos. Sci.*, **37**, 1313-1326.

Linden, P. F., 1975, The deepening of a mixed layer in a stratified fluid., *J. Fluid Mech.*, **71**, 385-405.

MacVean, M. K. and P. J. Mason, 1990: Cloud-top entrainment instability through small-scale mixing and its parameterization. *J. Atmos. Sci.*, **47**, 1012-1030.

Moeng, C.-H., S.-H., Shen, and D. A., Randall, 1992: Physical processes within the nocturnal stratus-topped boundary layer, *J. Atmos. Sci.*, **49**, 2384-2401.

Moeng, C.-H., P. P. Sullivan, and B. Stevens, 1998: Including radiative effects in an entrainment-rate formula for buoyancy-driven PBLs. *J. Atmos. Sci.*, in press.

Nicholls, S., 1984: The dynamics of stratocumulus: aircraft observations and comparisons with a mixed layer model. *Quart. J. Roy. Meteor. Soc.*, **110**, 783-820.

Nicholls, S., and J. Leighton, 1986: An observational study of the structure of stratiform cloud sheets: Part I. Structure. *Quart. J. R. Meteor. Soc.*, **112**, 431-460.

Nicholls, S., and J. D. Turton, 1986: An observational study of the structure of stratiform cloud sheets: Part II. Entrainment. *Quart. J. R. Met. Soc.*, **112**, 461-480.

Nicholls, S., 1989: The structure of radiatively driven convection in stratocumulus. *Quart. J. Roy. Meteor. Soc.*, **115**, 487-511.

Paluch, I. R., and D. H. Lenschow, 1991: Stratiform cloud formation in the marine boundary layer. *J. Atmos. Sci.*, **48**, 2141-2158.

Penc, R. S., and B. A. Albrecht, 1987: Parametric representation of heat and moisture fluxes in cloud-topped mixed layers. *Bound.-Layer Meteor.*, **38**, 225-248.

Randall, D. A., 1980: Conditional Instability of the first kind upside-down. *J. Atmos. Sci.*, **37**, 125-130.

Siems, S. T., C. S. Bretherton, M. B. Baker, S. Shy, and R. T. Breidenthal, 1990: Buoyancy reversal and cloudtop entrainment instability. *Quart. J. Roy. Meteor. Soc.*, **116**, 705-739.

Stull, R. B., 1988: *An Introduction to Boundary Layer Meteorology*, Kluwer Academic Publishers, Dordrecht, The Netherlands.

Turner, J. S., 1973: *Buoyancy Effects in Fluids*, Cambridge University Press.

Wang, Q., 1993: Turbulent mixing and transport in marine stratocumulus-topped boundary layers--an observational study. Ph.D. dissertation, Department of Meteorology, The Pennsylvania state University, University Park, PA 199 pp.

Wang, Q., and B. A. Albrecht, 1994: Observations of cloud-top entrainment in marine stratocumulus clouds. *J. Atmos. Sci.*, **51**, 1530-1547.

Wang, Q., D. H. Lenschow, L. Pan, R. D. Schillawski, G. L. Kok, A. S. H. Prevot, K. Laursen, L. M. Russel, A. Bandy, D. Thornton, and K. Suhre, 1998: Characteristics of the Marine Boundary Layers During Two Lagrangian Measurement Periods, Part II: Turbulence Structure. Submitted to *Journal of Geophysical Research*, 14 January 1998.

INITIAL DISTRIBUTION LIST

	No. Copies
1. Defense Technical Information Center..... 8725 John J. Kingman Road, STE 0944 Ft. Belvoir, Virginia 22060-6218	2
2. Dudley Knox Library..... Naval Postgraduate School 411 Dyer Rd. Monterey, California 93943-5101	2
3. Chairman, Code MR..... Department of Meteorology Naval Postgraduate School Monterey, California 93943-5101	1
4. Chairman, Code OC..... Department of Oceanography Naval Postgraduate School Monterey, California 93943-5101	1
5. Professor Qing Wang, Code MR/Qg..... Naval Postgraduate School Monterey, California 93943-5101	3
6. Professor Robert Haney, Code MR/Hy..... Naval Postgraduate School Monterey, California 93943-5002	1
7. Commander..... Naval Meteorology and Oceanography Command 1020 Bach Boulevard Stennis Space Center, Mississippi 39529-5005	1
8. LCDR David W. McDowell..... NAVEURMETOCEN Rota, Spain PSC 819 Box 31 FPO AE 09645-3200	2